ANALYTICAL STUDY OF A TECHNIQUE FOR THE ELIMINATION OF STEERING RATE GYRO BIAS IN A TYPICAL MISSILE AUTOPILOT

by

ROBERT CLAYTON ESLINGER

B. S., Kansas State University
of Agriculture and Applied Science, 1962

A MASTER'S REPORT

submitted in partial fulfillment of the

requirements for the degree

MASTER OF SCIENCE

Department of Electrical Engineering

KANSAS STATE UNIVERSITY
Manhattan, Kansas

1963

Approved by:

C.H. Mumick

Major Professor

TABLE OF CONTENTS

INTRODUCTION.....1

DEVELOPMENT OF A TYPICAL AUTOPILOT.....2

STEADY STATE BIAS INTRODUCTION.....17

ANALYTICAL APPROACH TO BIAS ELIMINATION STUDY.....18

ANALOG SIMULATION APPROACH TO BIAS ELIMINATION STUDY.....30

CONCLUSION.....36

ACKNOWLEDGMENT.....48

INTRODUCTION

In recent years both manned and unmanned aircraft have come to play an important role in our society. Because of this role more and more emphasis has been placed on the improvement of these vehicles. One field wherein advancements have excelled is the missile field where the early trial and error methods of analysis and synthesis have yielded to predictable methods utilizing analog and digital computers and today we can boast of ICBM's capable of tremendous tasks. This thesis will be concerned with a typical missile control loop and the possibility of an improvement of this loop.

In many missile autopilots rate gyro feedback is used to help stabilize the system. Associated with the rate gyro is a steady state bias which can be large enough to have a pronounced effect on missile performance. This bias will vary, of course, with the quality of gyro but if an inexpensive means could be developed to alleviate the bias problem considerable savings could be effected through the use of lower quality gyros.

The purpose of this thesis will be to show a means of decoupling this gyro bias and then to investigate the system to make sure missile autopilot performance is not depreciated significantly. Several means are employed as a determination of missile performance. One such means is the investigation of rate feedback open loop margins and another is the analysis of the transient response of the system (i.e. for a step input it is desireable to achieve a good approximation to a step output).

Before the system can be analyzed and understood a development

of a typical autopilot will first be undertaken. The analysis will then be accomplished by making an analytical study of the system and then making an analog study of the same system.

DEVELOPMENT OF A TYPICAL AUTOPILOT[1]

The functional block diagram of a typical guided missile system is shown in Figure 1. In any such system the target and missile position are compared and the resultant guidance error signal is fed to the missile control system which in turn acts to null the error signal.

The guidance computer is used to provide the appropriate error signal and to provide a suitable missile lateral acceleration command. The missile autopilot, the unit which will be analyzed in this discussion, in turn accepts the acceleration command signal and activates the control surfaces as required to provide lateral acceleration. The component of lateral acceleration normal to the flight path acting in combination with the missile velocity produces a change in flight path angle so as to null the error between desired missile position in space and the actual position.

From Figure 1, it is seen that the autopilot plays a very important roll in the overall guidance loop. Likewise, the missile airframe characteristics determine to a large extent the autopilot responses.

---

[1] The development of the autopilot follows a procedure presented in several sets of notes used in Johns Hopkins University Applied Physics Laboratory's training program.

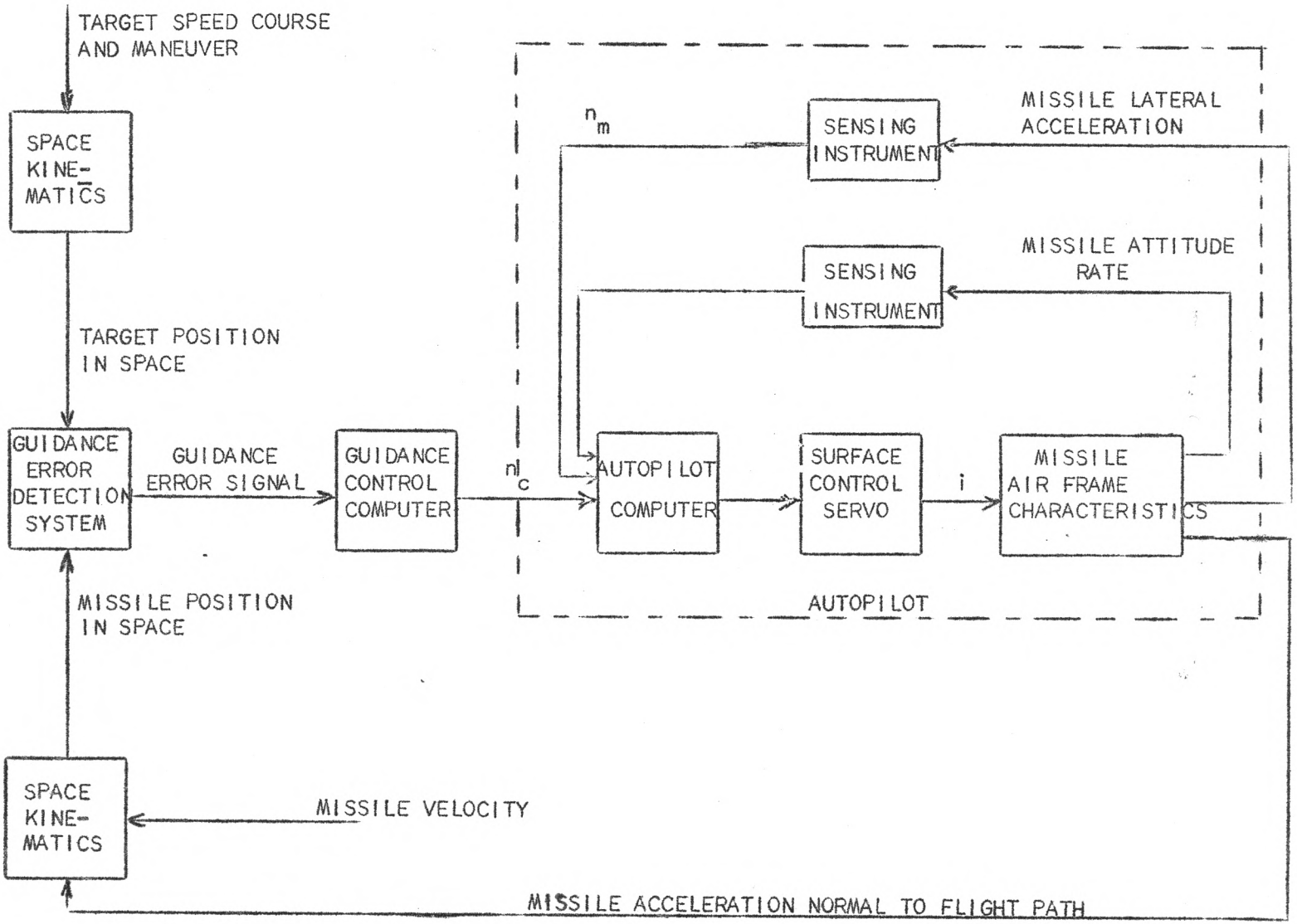

FIGURE 1. TYPICAL GUIDED MISSILE FUNCTIONAL BLOCK DIAGRAM

For this reason the autopilot is developed around these airframe characteristics since for any particular missile these characteristics will be deterministic.

The autopilot is actually a group of several distinct, though inter-related, systems designed to control the altitude and maneuvers of the airframe. The overall objective is to receive guidance commands and convert them into airframe maneuvers as quickly as possible under all conditions of flight with a minimum of overshoot.

The autopilot generally performs two functions, control of steering and roll. The treatment here will be limited to the steering autopilot or that part of the autopilot which acts to control the lateral maneuvers (pitch and yaw planes) of the airframe.

In practice, a variety of aerodynamic configurations may be employed. However, the underlying principles involved in the determination of specific dynamic characteristics (i.e. the aerodynamic transfer function) are identical. Only the "numbers" will vary.

In actual design practices for such a steering autopilot, Figure 2 can be used as a basic defining diagram for pitch angle relationships for one plane. An identical relationship will hold for the remaining plane and will be 90 degrees out of phase. C.P. is the center of pressure and is defined as that point on the missile airframe at which a single force may be thought to be concentrated which will exactly duplicate the effects of the distributed air pressure on the entire missile body and undeflected control surfaces.

C.G. is the center of gravity which may be thought of as the balance point for the distributed mass of the entire airframe. The angles are σ (angle-of-attack of the missile air frame with respect to the air stream), Σ (the angle between the air stream or velocity vector and an arbitrary inertial reference), and Θ (the angle between the airframe center-line and the same arbitrary inertial reference). Also defined are the sign convention for positive moment (M), positive lateral force (F), and positive control surface incidence (i).

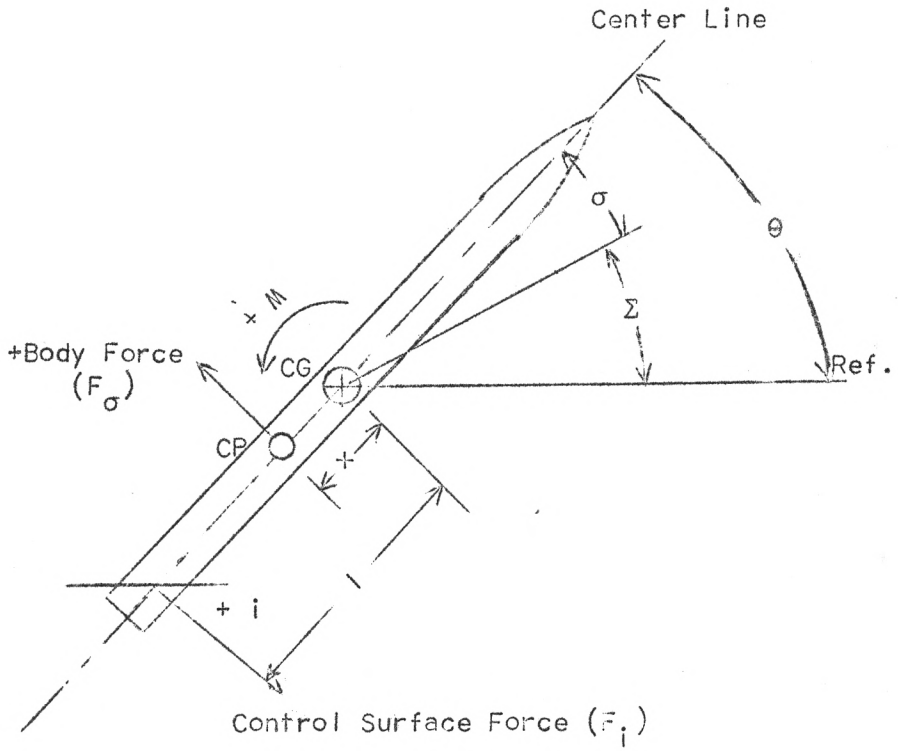

Figure 2. Missile Free Body Diagram In One Plane

In actual design procedures the designer has control over where the c.g. is placed (by actual design of the airframe and control surfaces). In selecting these two points one is faced with two conflicting desires. First of all it is desirable that the c.p. be positioned relative to the c.g. in such a way that the airframe is statically stable so that the task of the autopilot in stabilizing the airframe is as simple as possible. Conflicting with this desire, however, is the equally important consideration that the airframe not be so stable that high control moments are required to turn it. In other words, the designer is faced with a choice of highly stable, but difficult to maneuver vehicle or an unstable, but easy to maneuver vehicle. Generally, in the case of unmanned aircraft and missiles, the choice is made to keep the missile as near to neutral stability as possible providing a good compromise between these two conflicting requirements. For this situation the c.g. is designed to vary equally around the c.p. as fuel is burned and the position of the c.g. therefore changes.

All configurations may be thought of as made up of two basic elements, namely, the fixed portions of the configuration and the movable control surfaces. As the missile travels through the air at high velocity forces are produced on these two separate elements. The summation of these forces and the rotational moments they produce determine the aerodynamic response characteristics of the missile.

Figure 2 shows the basic force and moment representation of a missile. The total lateral force, equation (1), is comprised of F_σ and F_i . F_σ is the resultant force located at the center of pressure and is a representation of the lateral force due to the lift of the

air stream. F_i is the resultant force located at the tail and is a representation of the lateral force due to the control surfaces. Equation (2) is the moment equation which results from F_σ and F_i and their corresponding moment arms. These force and moment equations can now be represented by the block diagram in Figure 3.

$$F_T = F_\sigma + F_i \qquad (1)$$

$$M_T = M_\sigma + M_i = - F_\sigma \cdot x + F_i \cdot l \qquad (2)$$

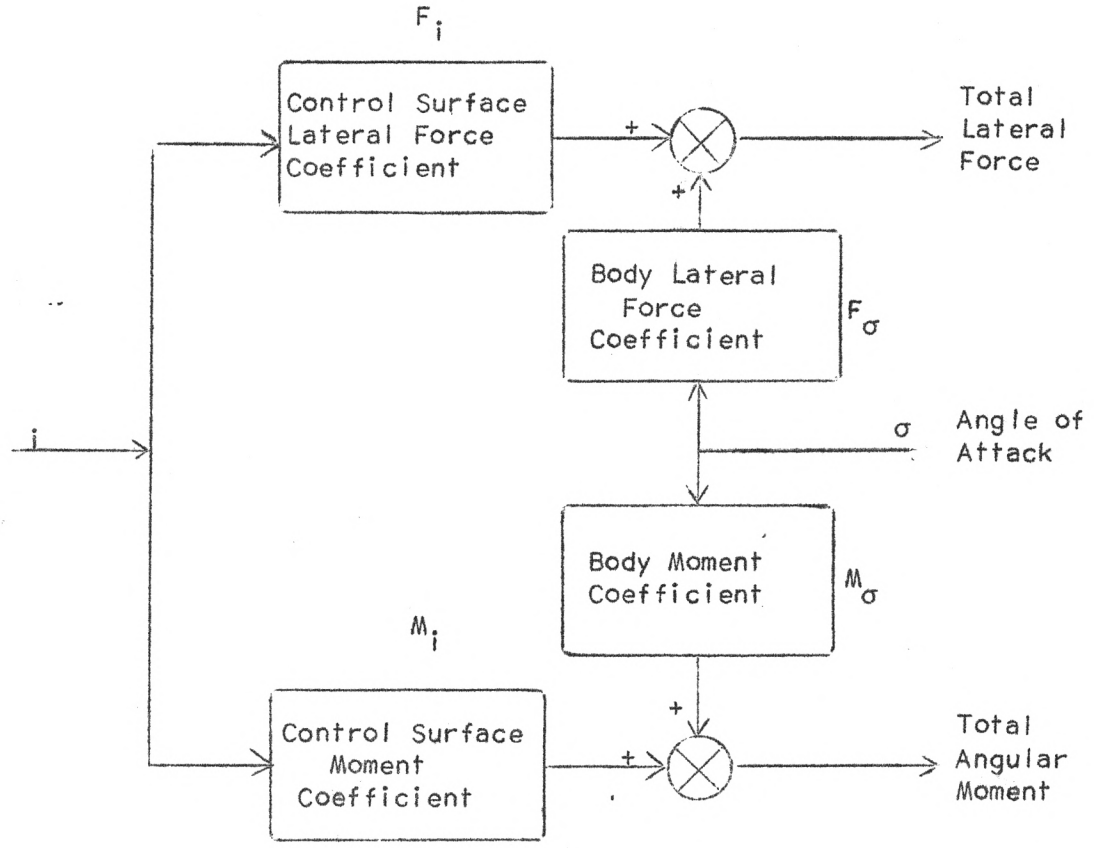

Figure 3. Summation of Missile Dynamics

The output of the moment summation may be thought of as a torque on the airframe which, if divided by the airframe moment of inertia, is converted into an angular acceleration in degrees per second squared. The output of the lateral force summation if divided by the mass of the missile, results in linear acceleration terms (ft./sec.^{2}) which in turn, if divided by g (32 ft./sec.^{2}), would result in lateral acceleration in g's. This summation system can be abbreviated in aerodynamic terminology according to the symbols in Figure 5 where

A = normal acceleration in g's per degree angle of attack

B = normal acceleration in g's per degree surface incidence

C = yaw rate in degrees per sec.^{2} per degree angle of attack

E = yaw rate in degrees per sec.^{2} per degree incidence

As shown in Figure 5 lateral acceleration, angle of attack, and body angular acceleration are not directly related. If a relationship between these three angular quantities could be derived then a closed block diagram of the aerodynamics could be formed.

From Figure 4 it is seen that the following relationships will hold (assuming constant forward velocity).

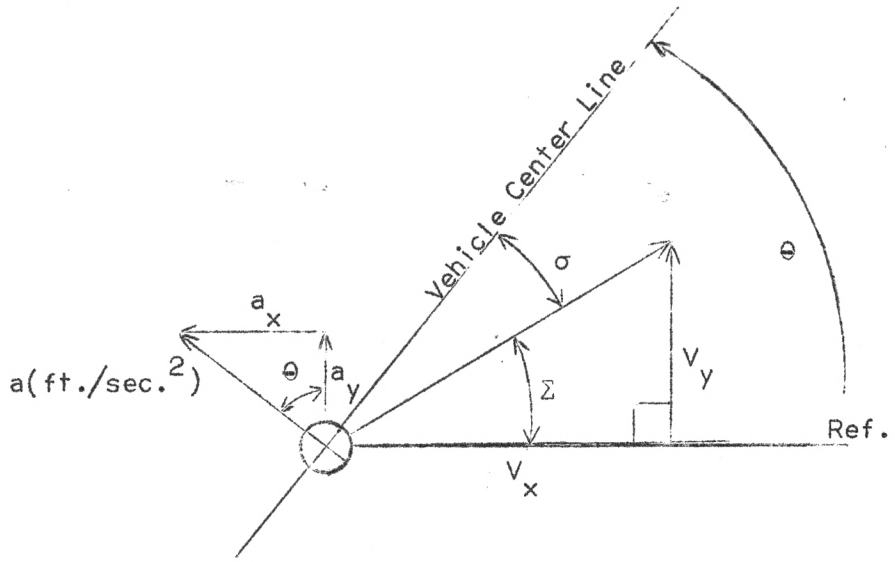

Figure 4. Missile Angular Relations

$$a_y = \dot{V}_y = a \cos \Theta \tag{3}$$

$$a_x = \dot{V}_x = - a \sin \Theta \tag{4}$$

$$V = V_x \cos \Sigma + V_y \sin \Sigma \tag{5}$$

$$\tan \Sigma = \frac{V_y}{V_x} = \frac{\sin \Sigma}{\cos \Sigma} \tag{6}$$

$$\text{or } V_x \sin \Sigma = V_y \cos \Sigma \tag{7}$$

differentiation yields

$$\dot{V}_x \sin \Sigma + V_x \dot{\Sigma} \cos \Sigma = \dot{V}_y \cos \Sigma - V_y \dot{\Sigma} \sin \Sigma \tag{8}$$

$$(V_x \cos \Sigma + V_y \sin \Sigma)\, \dot{\Sigma} = - \dot{V}_x \sin \Sigma + \dot{V}_y \cos \Sigma \tag{9}$$

$$\text{or } \dot{\Sigma} = \frac{a \sin \Theta \sin \Sigma + a \cos \Theta \cos \Sigma}{V} \tag{10}$$

$$\dot{\Sigma} = \frac{a \cos (\Theta - \Sigma)}{V} = \frac{a \cos \sigma}{V} \frac{\text{rad.}}{\text{sec.}} \tag{11}$$

$$\frac{\dot{\Sigma}}{a} = \frac{\cos \sigma}{V} \doteq \frac{1}{V} \frac{\text{rad./sec.}}{\text{ft./sec.}^2} \tag{12}$$

$$\frac{\dot{\Sigma}\ (\text{deg/sec.})}{a\ (\text{g's})} = \frac{57.3 \times 32.2}{V} = \frac{1845}{V} \frac{\text{deg./sec.}}{g} \tag{13}$$

$$= \bar{k} \tag{14}$$

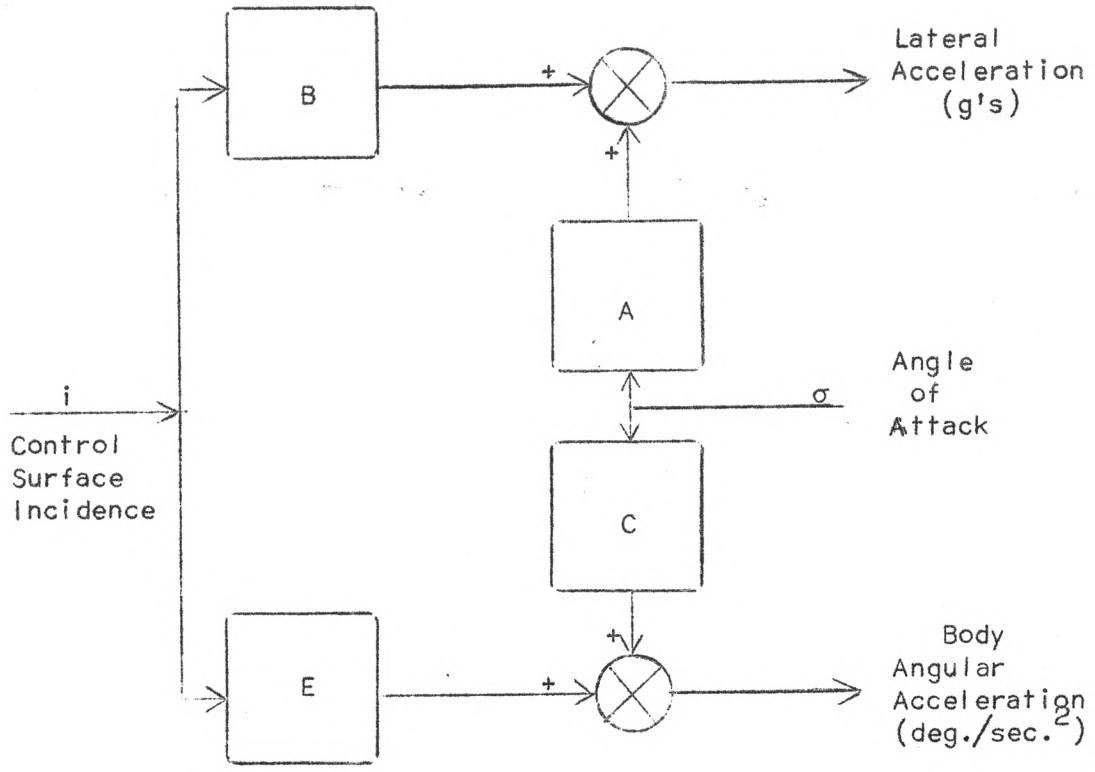

Figure 5. Summation of Missile Aerodynamics

Having determined the relationship between missile lateral acceleration and velocity vector turning rate ($\dot{\Sigma}$), the aerodynamic block diagram may now be completed with only simple integral relationships between angular rates and angles ($\dot{\theta} = \dot{\sigma} + \dot{\Sigma}$). The completed aerodynamic block diagram for the steering autopilot is shown in Figure 6.

Referring back to Figure 1 it can be seen that the block marked missile airframe characteristics has been developed. This expresses the relationship between control surface incidence and airframe variables. It is now left to consider the instrumentation of the actual system to force the airframe to perform in the prescribed manner.

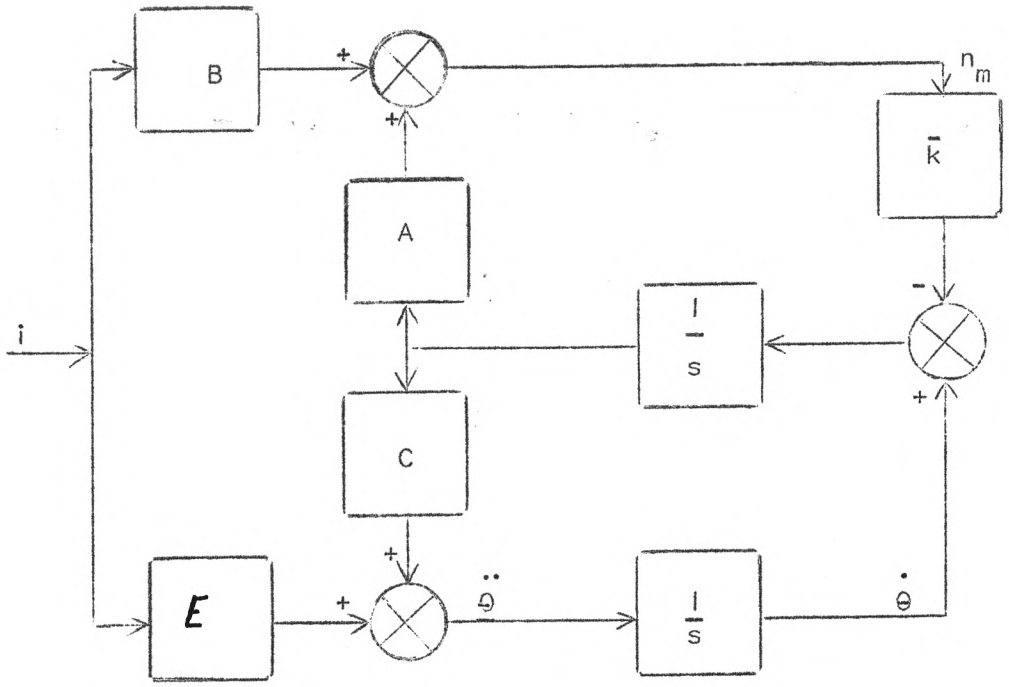

Figure 6. Aerodynamic Block Diagram For A Steering Autopilot

Since the guidance system requires that the velocity vector of the missile be rotated or, in other words, that the missile achieve lateral acceleration, it seems obvious that a feedback channel should be employed in the steering autopilot to sense the actual missile lateral acceleration for comparison with the acceleration that is being called for. In this way the autopilot can continually monitor how well it is satisfying the guidance system commands and take appropriate action if these quantities are not identical.

It can next be reasoned that it would be desirable to have high gain in the forward acceleration loop to minimize the difference between n_c, the required lateral acceleration, and n_m, the actual lateral acceleration.

High gain at all frequencies is not practical since it is necessary to have the loop gain low in the range of the aeroelastic natural frequency. The obvious answer is an integration which results in a high gain at low frequencies and a low gain at high frequencies. The transfer function (n_m / n_c) as developed for the solid line case in Figure 7 is:

$$\frac{n_m}{n_c} = \frac{\left(\frac{B}{D} s^2 + 1\right)}{\frac{s^3}{K_1 D} + \frac{K_1 B + \bar{K} A}{K_1 D} s^2 + \frac{-C}{K_1 D} s + 1} \qquad (15)$$

where $D = AE - BC$

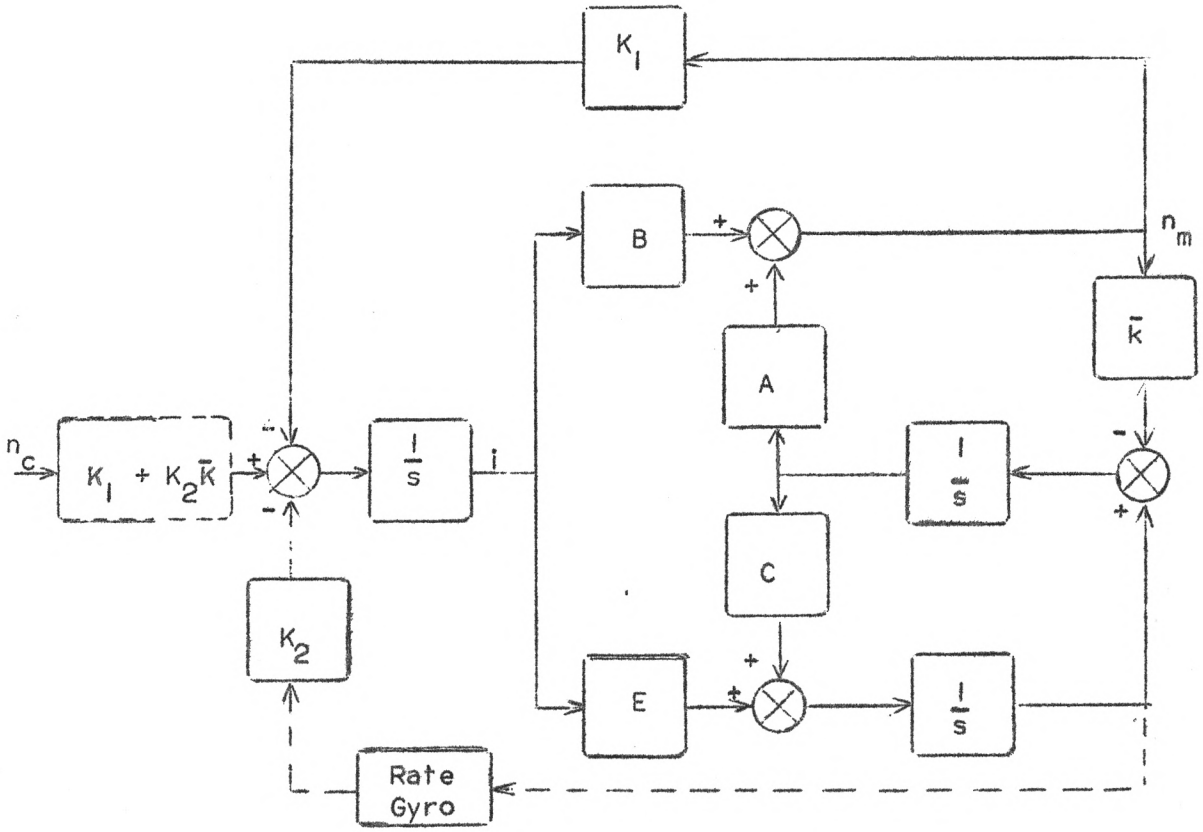

Figure 7. Partial Autopilot Block Diagram

It may be recalled from the Routh stability criterion that in order for this transfer function to represent a stable system, all of the coefficients of the denominator must be of the same sign. Investigation of the coefficients of the "s" term will lead one to the conclusion that in the presense of an unstable airframe (positive C), this coefficient will be negative and the overall autopilot transfer function will be unstable.

If an angular rate gyro is mounted on the airframe and connected into the acceleration summing junction as shown in Figure 7 (solid lines plus dashed lines), the autopilot closed loop transfer function becomes:

$$\frac{n_m}{n_c} = \frac{\left(\frac{B}{D}s^2 + 1\right)}{\frac{s^3}{(K_1 + K_2\bar{K})D} + \frac{K_1B + \bar{K}A}{(K_1 + K_2\bar{K})D}s^2 + \frac{K_2E - C}{(K_1 + K_2\bar{K})D}s + 1} \qquad (16)$$

This addition of the rate gyro output signal to the autopilot through a gain K_2 results in a term added to the coefficient of "s", K_2E, which can be made large enough to hold the coefficient positive in the presence of the most unstable variation of the static stability parameter C.

In actual missile instrumentation this rate gyro has a steady state bias which leads to difficulties. The elimination of this bias and the effects the decoupling will have on the overall system will be the main subject of this thesis.

Even with the addition of the rate gyro the problem of stability is not entirely solved. Even though the coefficient of the "s" term is now positive, the coefficient of "s^2" can be negative through the influence of B. The addition of the rate gyro derivative through a gain K_3 will result in an improvement of the coefficient of "s^2" as shown in the following transfer function as derived from Figure 8.

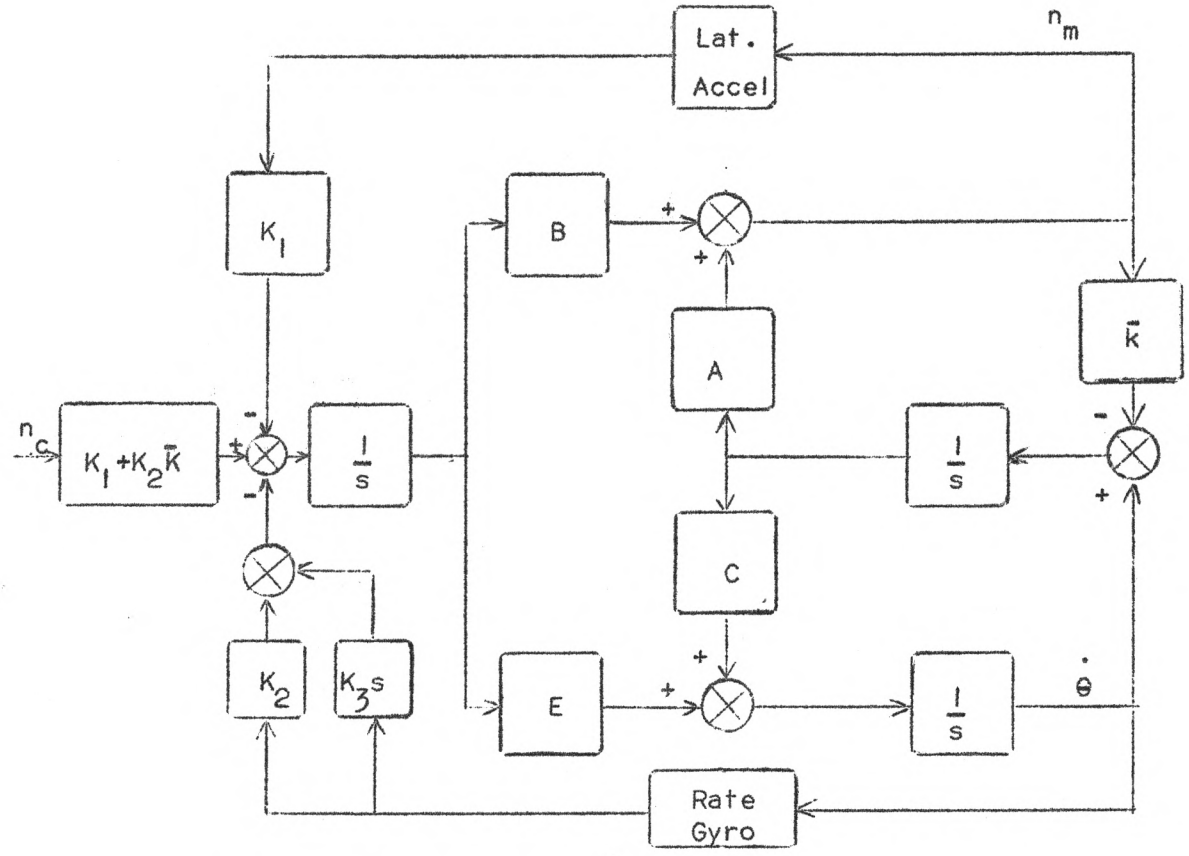

Figure 8. Complete Autopilot Block Diagram

$$\frac{n_m}{n_c} = \frac{\left(\frac{B}{D}s^2 + 1\right)}{\frac{s^3}{(K_1 + K_2\bar{K})D} + \frac{K_1B + \bar{K}A + K_3E}{(K_1 + K_2\bar{K})D}s^2 + \frac{K_2E - C + K_3\bar{K}D}{(K_1 + K_2\bar{K})D}s + 1} \qquad (17)$$

Inspection of this final transfer function reveals that all the denominator coefficients are now held positive by appropriate autopilot gains.

In the development thus far it has been implied that if the airframe static stability can be handled, the autopilot design will be safe. This is not quite the case. In reality, there are a number of instrument lags in the system which create an additional stability problem in the control system. This possible instability is best seen if the rate gyro channel of the autopilot is broken and an open loop response check made at this point. A typical Bode plot with no consideration of lags (solid lines) and with the lags considered (dotted lines) is shown in Figure 9.

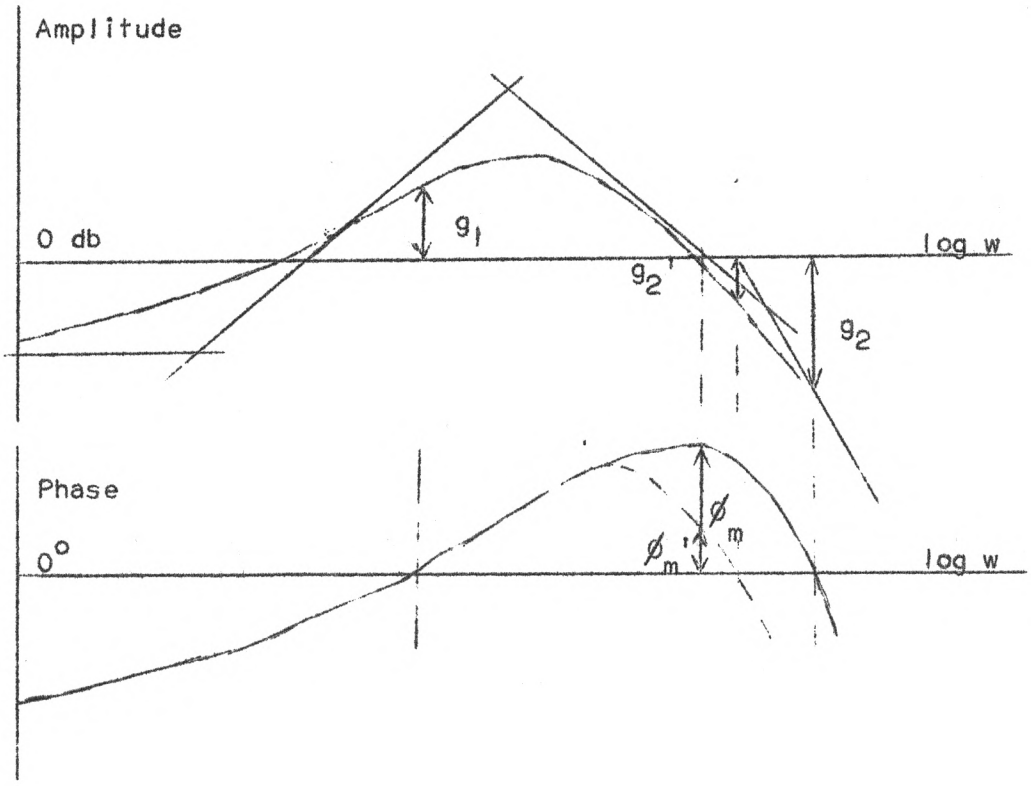

It can be seen that the high frequency gain margin (HFGM) and the phase margin (ϕ_m) will decrease when the phase lags are considered. There are three frequencies of interest where a gain change or an extraneous lag will cause the system to become unstable; g_1 is known as the low frequency gain margin (LFGM), ϕ_m is known as the phase margin, and g_2 is known as the high frequency gain margin mentioned above. This thesis will pay very close attention to these margins since they will show very quickly any effect which will tend to cause a system to become unstable.

As a missile flies from its launching position into higher altitudes, it experiences a considerable variation in aerodynamic pressure. This variation affects directly the aerodynamic parameters, A, B, and E. To compensate for these wide variations, the gains, K_1, K_2, and K_3 in the missile must be varied in some manner that is proportional to altitude. This thesis will consider analysis only at the two extreme altitudes that the missile will experience and assume that all other conditions will fall between the low altitude and high altitude cases.

The previous discussion presents a very basic introduction to a linear autopilot development. It is given here merely as a necessary introduction to the actual problem development to follow.

STEADY STATE BIAS INTRODUCTION

The basic steering autopilot development is summarized in Figure 8. A summing junction block diagram redrawn from this figure is shown in Figure 10. For steady state conditions and no input (Figure 11), there should be no output from the summing junction. If an output exists the autopilot would see a call for lateral acceleration (n_c) and would deflect the tail surfaces correspondingly. For no output to exist from the summing junction equation 18 must hold.

$$n_m = \frac{K_2}{K_1} \dot{\theta}_b \tag{18}$$

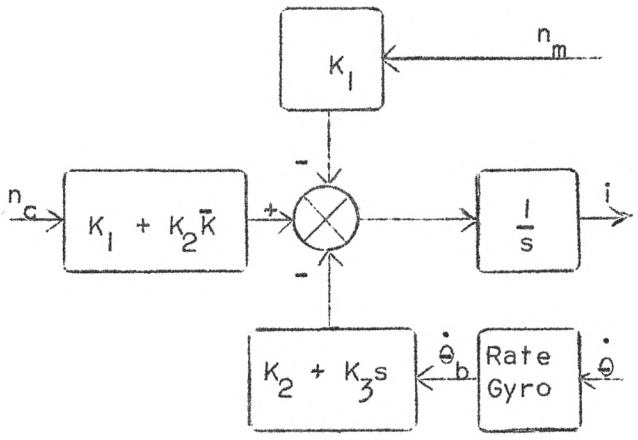

Figure 10. Summing Junction Diagram of Basic Autopilot

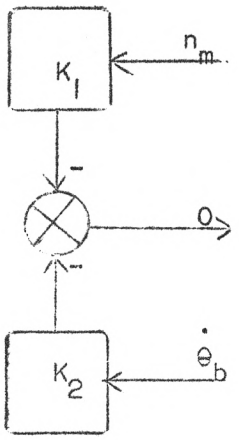

Figure 11. Summing Junction Diagram For Steady State Conditions

A typical value for this gyro bias ($\dot{\theta}_b$) could be of the order of 1° per second. For low altitude conditions and typical values of K_2 and K_1 (obtained from Table I) of 2.5 and 3.0, respectively, n_m would have a value of 0.833 g's. At high altitudes this value is reduced to 0.0933 g's.[1]

Practically this is a situation where the control surfaces are actually deflected due to the n_m bias when no acceleration (n_c) is being called for. Obviously this is an undesireable condition and one that should be eliminated or at least minimized.

ANALYTICAL APPROACH TO BIAS ELIMINATION STUDY

The block diagram of the basic acceleration feedback autopilot is shown in Figure 12. The servo and rate gyro high frequency characteristics, $F_1(s)$ and $F_2(s)$ respectively, have been assumed to be damped second order functions with a damping constant of $\frac{1}{2}$ and a corner frequency of 130 radians per second for the servo and 325 radians per second for the rate gyro.

Due to the fact that the airframe is an elastic device subject to perturbations as it flies through the air, filtering must be included in the autopilot to preclude the possibility of an oscillation throughout the control system due to the control surfaces reinforcing the self-induced body oscillations. For this reason, notch filters are included in the autopilot to attenuate any body mode activity which may be sensed by the rate gyro derivative channel. These filters are simply represented by a

---

[1] Not actually representative of present "state of the art" values but reasonable values for a physical vehicle.

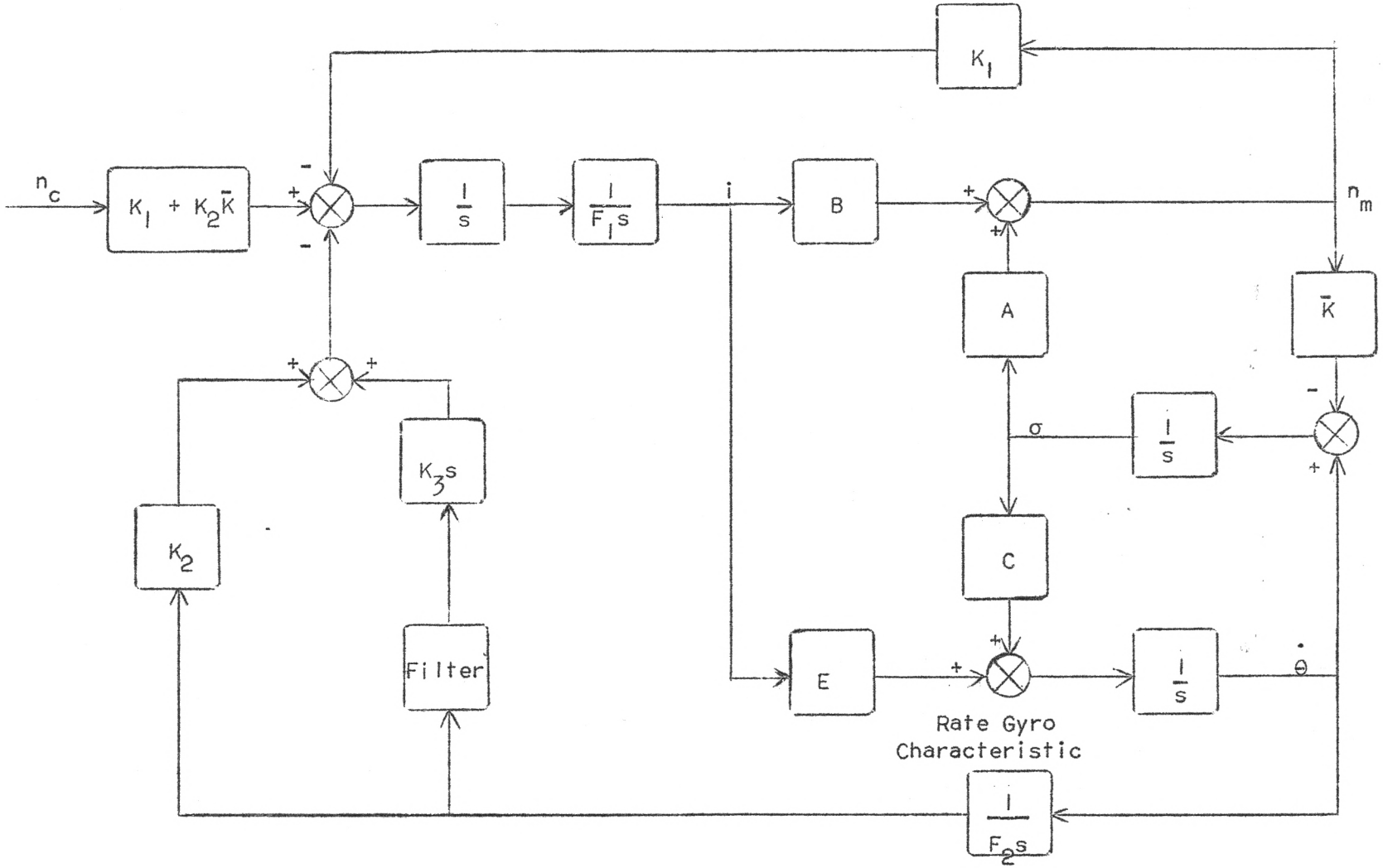

Figure 12. Basic Acceleration Feedback Autopilot

basic lag network $\frac{1}{T_1 s + 1}$.

The basic criterion for this study shall be as follows:

1. Autopilot rate loop margins shall not be diminished by more than 1 db or 5°.
2. Total rate gyro drift bias rejection is required.
3. The transient-response of n_m shall maintain not more than 20% overshoot.
4. Attention will be given to the rise time and time required to reach final value.

Due to the relatively low frequency nature of the acceleration feedback loop, the effect produced by the high frequency servo characteristic on this loop can be ignored. For analysis purposes, the servo characteristic, $F_1(s)$ is considered only as it affects the rate feedback signals. Likewise for analysis purposes the $\dot{\theta}$ feedback loop will be opened and the margins investigated at this point. The $\dot{\theta}$ feedback loop was chosen since it is regarded as the most sensitive loop and therefore would tend to show a trend toward instability more readily.

The diagram for the $F_1(s)$ approximation and with the $\dot{\theta}$ feedback loop opened is shown in Figure 13.

From Figure 13 the transfer function for $\dot{\theta}_m / \dot{\theta}_e$ can be found to be,

$$\frac{\dot{\theta}_m}{\dot{\theta}_e} = \frac{-\frac{K_2 \bar{K}}{K_1}\left[\frac{E}{\bar{K}D}s + 1\right]\left[\frac{K_3}{K_2(T_1 s + 1)}s + 1\right]}{\left[\frac{s^3}{K_1 D} + \frac{K_1 B + \bar{K}A}{K_1 D}s^2 - \frac{C}{K_1 D}s + 1\right] F_1(s)\, F_2(s)} \qquad (19)$$

where $D = AE - BC$

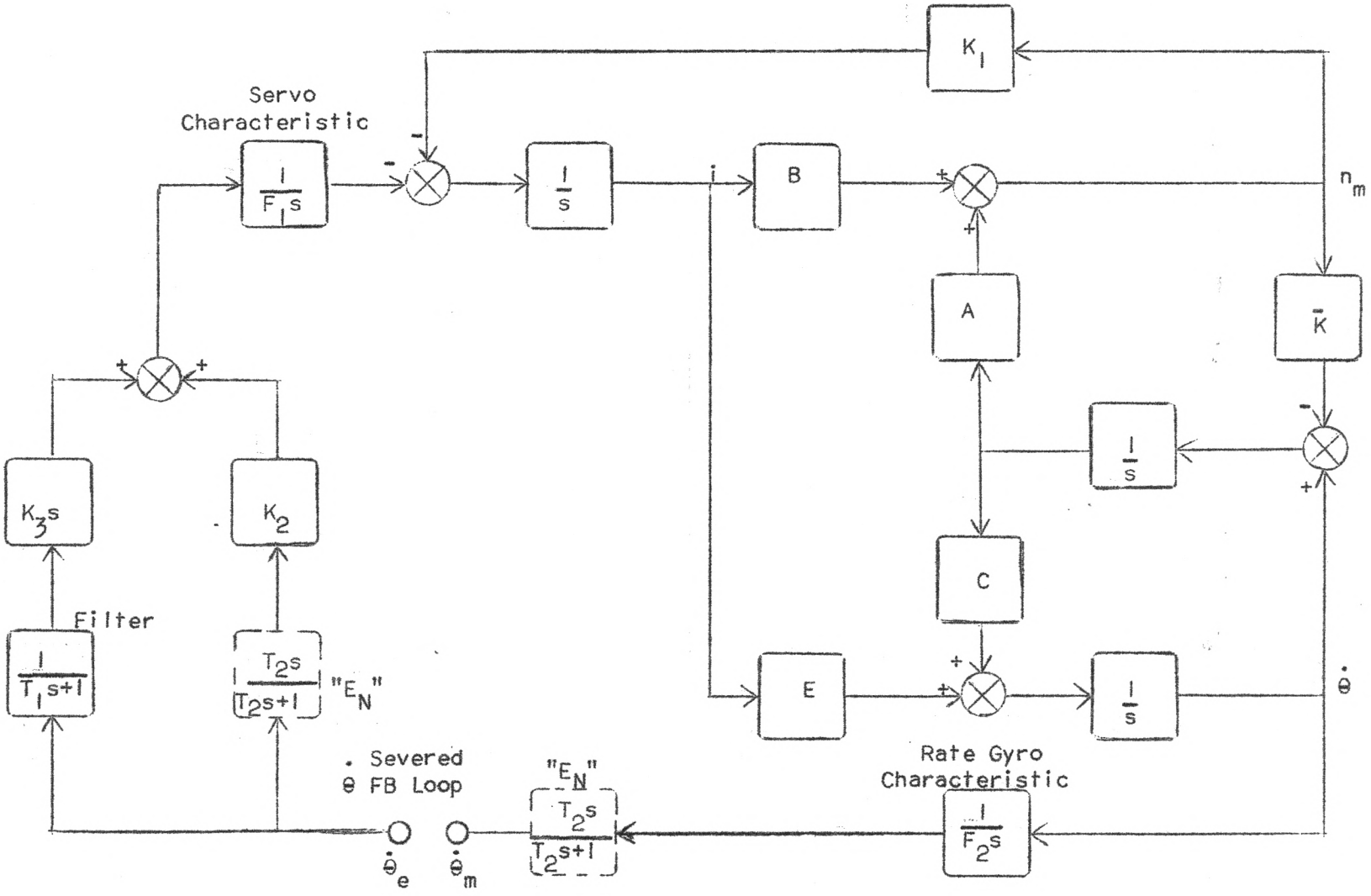

Figure 13. Simplified Autopilot With Two Possible Locations for "E_N"

This equation will be evaluated at two extreme conditions of low altitude and high altitude. Typical values for the required parameters at the two extreme conditions are listed in Table I.

Table I. High and Low Altitude Autopilot Parameters

Parameter	L.A.	H.A.
A	5	0.2
B	-0.5	-0.02
C	70	7.5
E	200	7.5
$\bar{K}$	0.6	0.5
K_1	3	150
K_2	2.5	14
K_3	0.15	2.5
T_1	0.005	0.01

It is interesting to note here the difference in values. A, B, and E will change approximately the same percentage for the two conditions. This is as expected since these are all aerodynamic properties and are primarily proportional to dynamic pressure and therefore altitude. C, an aerodynamic parameter also, is dependent on more items than altitude one of which is the center of gravity and would not be expected to change correspondingly. $\bar{K}$ is inversely related to the missile velocity and therefore would be expected to decrease. The gains K_1, K_2, and K_3 would have to increase to keep the gain of the overall autopilot as sensitive to command at high altitudes as they were at low altitudes. The T_1 corner frequency decreases due to increased filtering and thus increased lag. These observations may give some insight to the system as analysis proceeds.

The undesireable rate gyro bias exists immediately following $F_2(s)$; therefore, the elimination of this bias can be accomplished by the addition of a decoupling block in the $\dot{\theta}$ feedback loop, immediately following $F_2(s)$, hereafter referred to as the $F_2(s)$ leg, or by the addition of a decoupling block in the K_2 leg. Both situations are as shown in Figure 13. The original system is understood to be the case where no decoupling blocks are present.

No decoupling block would be necessary in the K_3 leg since a differentiation is associated with this leg. The decoupling block can be represented by $T_2 s \,/\, (T_2 s + 1)$, a basic high pass filter, hereafter referred to as "E_N".

The analysis will consider both locations of "E_N" and will attempt to show which location would be the most desireable. The resulting transfer function for the consideration of "E_N" in the $F_2(s)$ leg is

$$\frac{\dot{\theta}_m}{\dot{\theta}_e} = \frac{-\frac{K_2\bar{K}}{K_1}\left[\frac{E}{\bar{K}D}s + 1\right]\left[\frac{K_3 + K_2T_1}{K_2}s + 1\right]}{\left[\frac{s^3}{K_1D} + \frac{K_1B + \bar{K}A}{K_1D}s^2 + \frac{-C}{K_1D}s + 1\right]\left[T_1s + 1\right]\left[T_2s + 1\right]F_1(s)\,F_2(s)} \tag{20}$$

where $F_1(s)$ and $F_2(s)$ are represented by

$$F_1(s) = \left[\frac{s^2}{(130)^2} + \frac{2(0.5)}{130}s + 1\right]$$

$$F_2(s) = \left[\frac{s^2}{(325)^2} + \frac{2(0.5)}{325}s + 1\right]$$

Evaluation of Equation 20 yields Equations 21 and 22.

Low Altitude

$$\frac{\dot{\theta}_m}{\dot{\theta}_e} = \frac{-0.5\left[\frac{s}{3.1}+1\right]\left[\frac{s}{15.35}+1\right]T_2 s}{\left[\frac{s^2}{(13.6)^2}-\frac{2(0.56)}{13.6}s+1\right]\left[\frac{s}{16.75}+1\right]\left[\frac{s}{200}+1\right]\left[T_2 s+1\right]F_1(s)\,F_2(s)} \tag{21}$$

High Altitude

$$\frac{\dot{\theta}_m}{\dot{\theta}_e} = \frac{-0.0466\left[\frac{s}{0.11}+1\right]\left[\frac{s}{5.3}+1\right]T_2 s}{\left[\frac{s^2}{(6.52)^2}-\frac{2(0.66)}{6.52}s+1\right]\left[\frac{s}{5.76}+1\right]\left[\frac{s}{100}+1\right]T_2 s+1\;\;F_1(s)\,F_2(s)} \tag{22}$$

The resulting transfer function for the consideration of "E_N" in the K_2 leg is

$$\frac{\dot{\theta}_m}{\dot{\theta}_e} = \frac{-\frac{K_2\bar{K}}{K_1}\left[\frac{T_2 s}{T_2 s+1}\right]\left[\frac{E}{\bar{K}D}s+1\right]\left[\frac{K_3(T_2 s+1)}{K_2(T_1 s+1)(T_2 s)}s+1\right]}{\left[\frac{s^3}{K_1 D}+\frac{K_1 B+\bar{K}A}{K_1 D}s^2-\frac{C}{K_1 D}s+1\right]\;\;F_1(s)\;\;F_2(s)} \tag{23}$$

which yields

$$\frac{\dot{\theta}_m}{\dot{\theta}_e} = \frac{-\frac{\bar{K}}{K_1}(K_3+K_2T_2)s\left[\frac{E}{\bar{K}D}s+1\right]\left[\frac{K_3T_2+K_2T_2T_1}{K_3+T_2K_2}s+1\right]}{\left[\frac{s^3}{K_1 D}+\frac{K_1 B+\bar{K}A}{K_1 D}s^2-\frac{C}{K_1 D}+1\right]\left[T_1 s+1\right]\left[T_2 s+1\right]F_1(s)\,F_2(s)} \tag{24}$$

Evaluation of Equation 24 for a value of $T_2 = 1.43$ yields Equations 25 and 26.

Low Altitude

$$\frac{\dot{\theta}_m}{\dot{\theta}_e} = \frac{-0.746\, s \left[\frac{s}{3.1} + 1\right]\left[\frac{s}{16.0} + 1\right]}{\left[\frac{s^2}{(13.6)^2} - \frac{2(0.56)}{13.6} s + 1\right]\left[\frac{s}{16.75} + 1\right]\left[\frac{s}{200} + 1\right]\left[T_2 s + 1\right] F_1(s)\, F_2(s)} \qquad (25)$$

High Altitude

$$\frac{\dot{\theta}_m}{\dot{\theta}_e} = \frac{-0.075\, s \left[\frac{s}{0.22} + 1\right]\left[\frac{s}{5.98} + 1\right]}{\left[\frac{s^2}{(6.52)^2} - \frac{2(0.664)}{6.52} s + 1\right]\left[\frac{s}{5.76} + 1\right]\left[\frac{s}{100} + 1\right]\left[T_2 s + 1\right] F_1(s)\, F_2(s)} \qquad (26)$$

For analysis purposes Bode plots for Equations 21, 22, 25, and 26 are drawn. Figure 14 shows the low altitude condition for no consideration of "E_N", (in other words for the uncompensated system) and the situation for "E_N" in the $F_2(s)$ leg with $T_2 = 1.43$. Figure 15 shows the situation for "E_N" in the K_2 leg with $T_2 = 1.43$. Figures 16 and 17 are a repeat of these situations for high altitude conditions. Comparison of the margins and respective frequencies tabulated in Table 2 shows very little difference for the addition of "E_N".

This value of T_2 was determined by analog computation as will be shown in the next section and was verified here by a Bode plot analysis.

From the preceding analysis it would appear that a T_2 of 1.43 or a first order corner frequency of 0.6 radians per second would

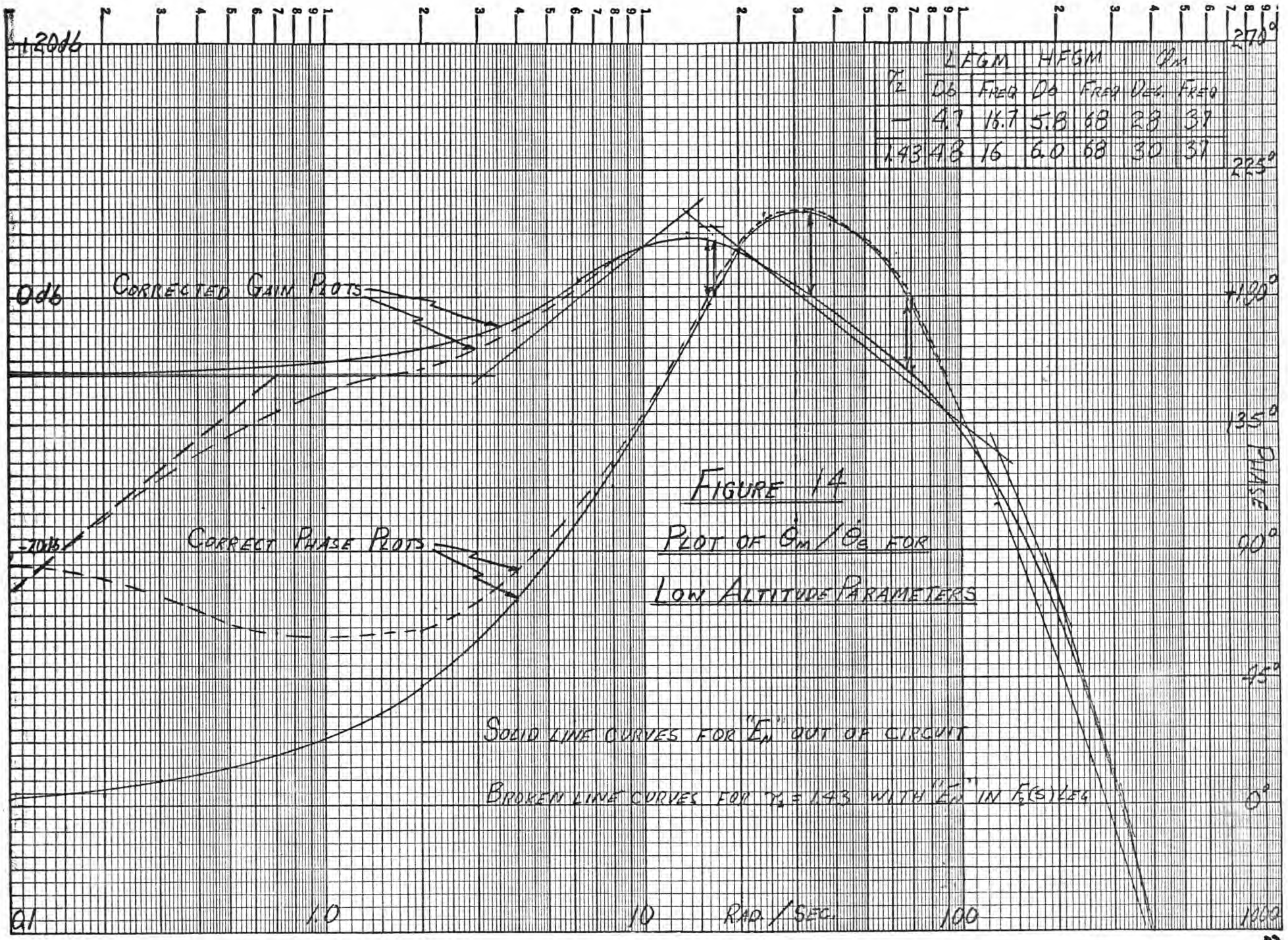

FIGURE 14

PLOT OF θ_M / θ_E FOR

LOW ALTITUDE PARAMETERS

SOLID LINE CURVES FOR "E_M" OUT OF CIRCUIT

BROKEN LINE CURVES FOR $T_2 = 1.43$ WITH "E_M" IN $F_2(S)$ LEG

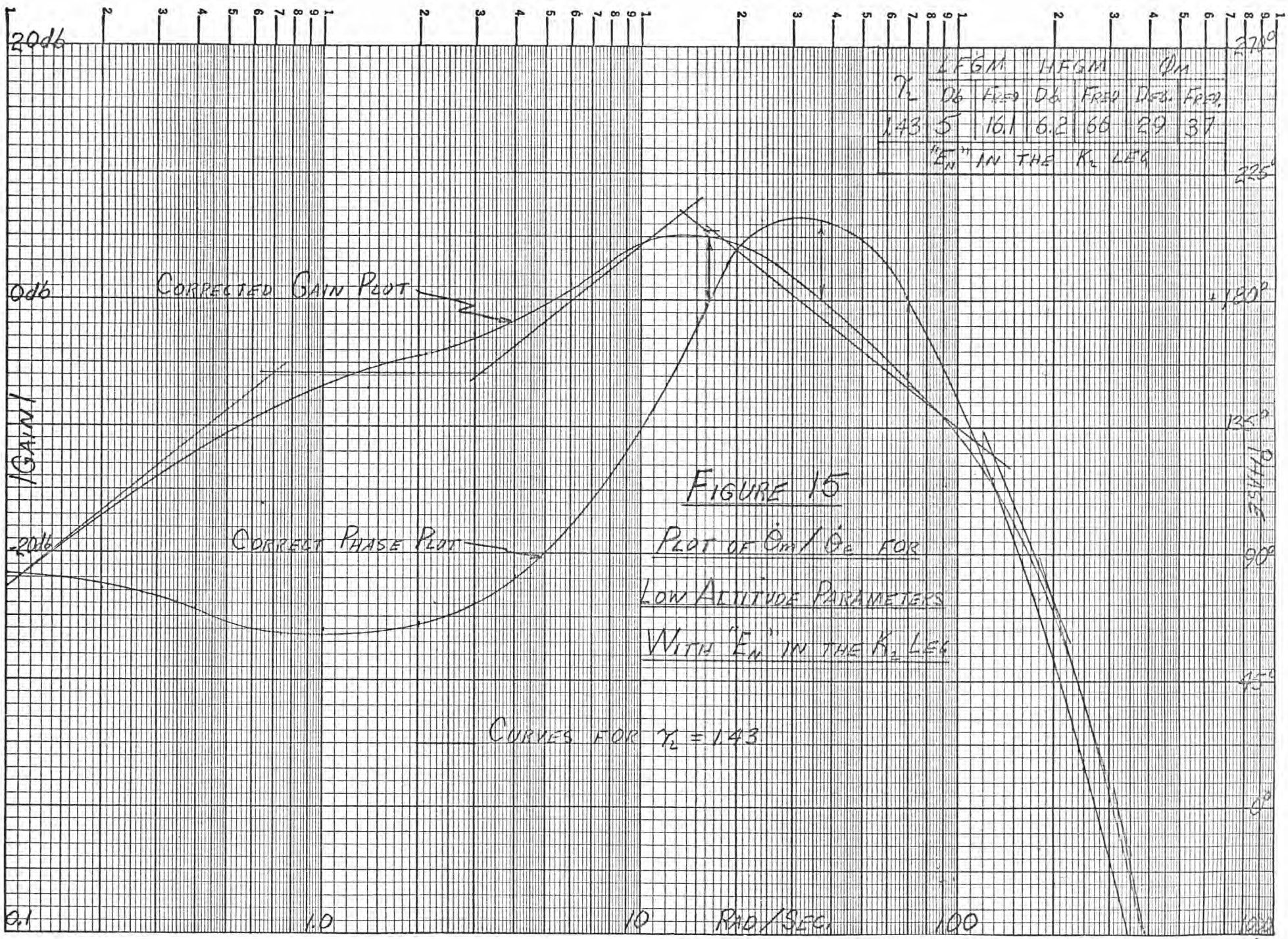

FIGURE 15

PLOT OF $\dot{\theta}_m / \dot{\theta}_c$ FOR LOW ALTITUDE PARAMETERS WITH "E_N" IN THE K_2 LEG

CURVES FOR $\gamma_2 = 1.43$

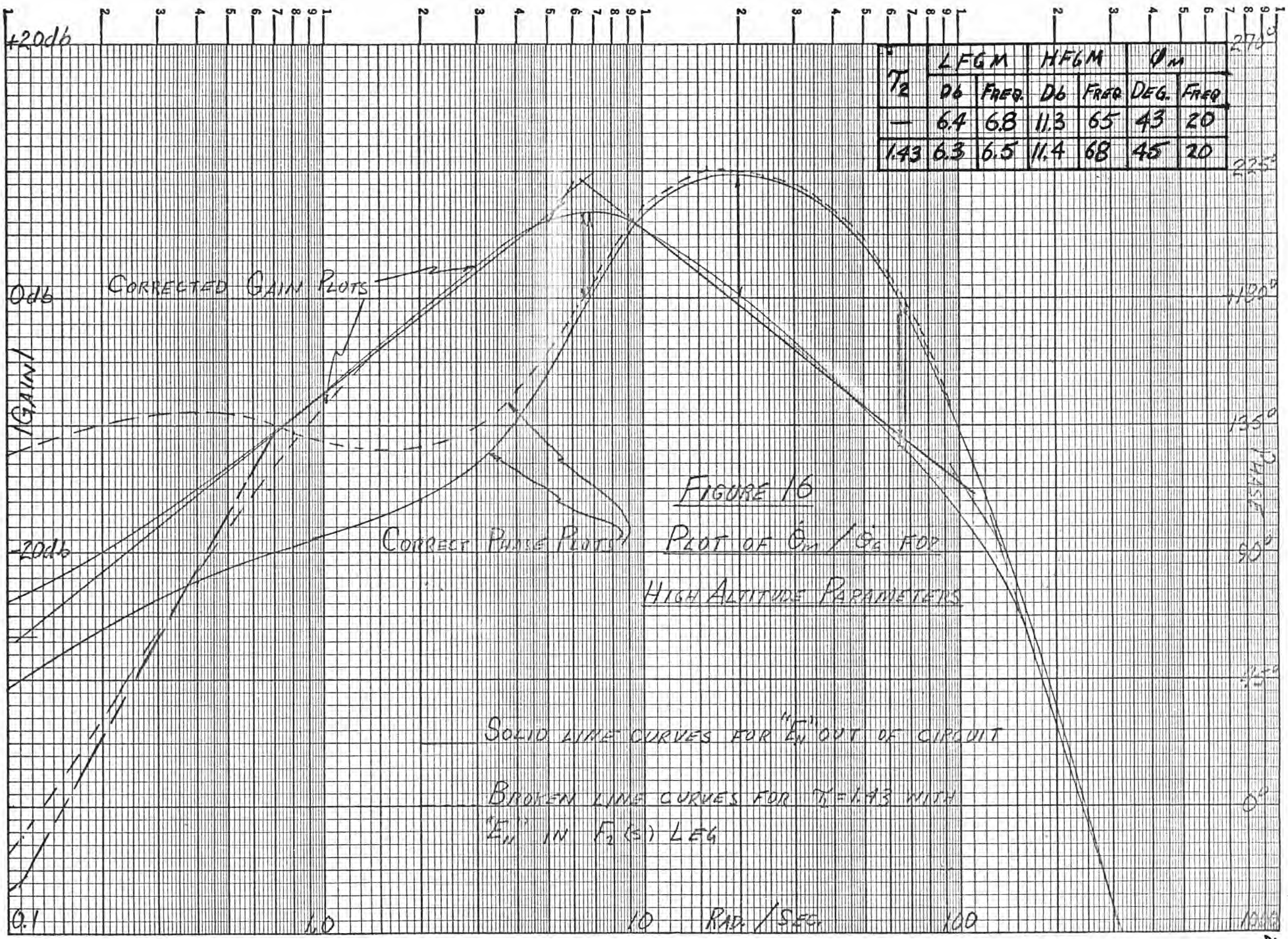

T_2	LFGM		HFGM		θ_M	
	DB	FREQ.	DB	FREQ	DEG.	FREQ
—	6.4	6.8	11.3	65	43	20
1.43	6.3	6.5	11.4	68	45	20

FIGURE 16

PLOT OF θ_M / θ_E FOR HIGH ALTITUDE PARAMETERS

SOLID LINE CURVES FOR "E_M" OUT OF CIRCUIT

BROKEN LINE CURVES FOR $T_2 = 1.43$ WITH "E_M" IN $F_2(s)$ LEG

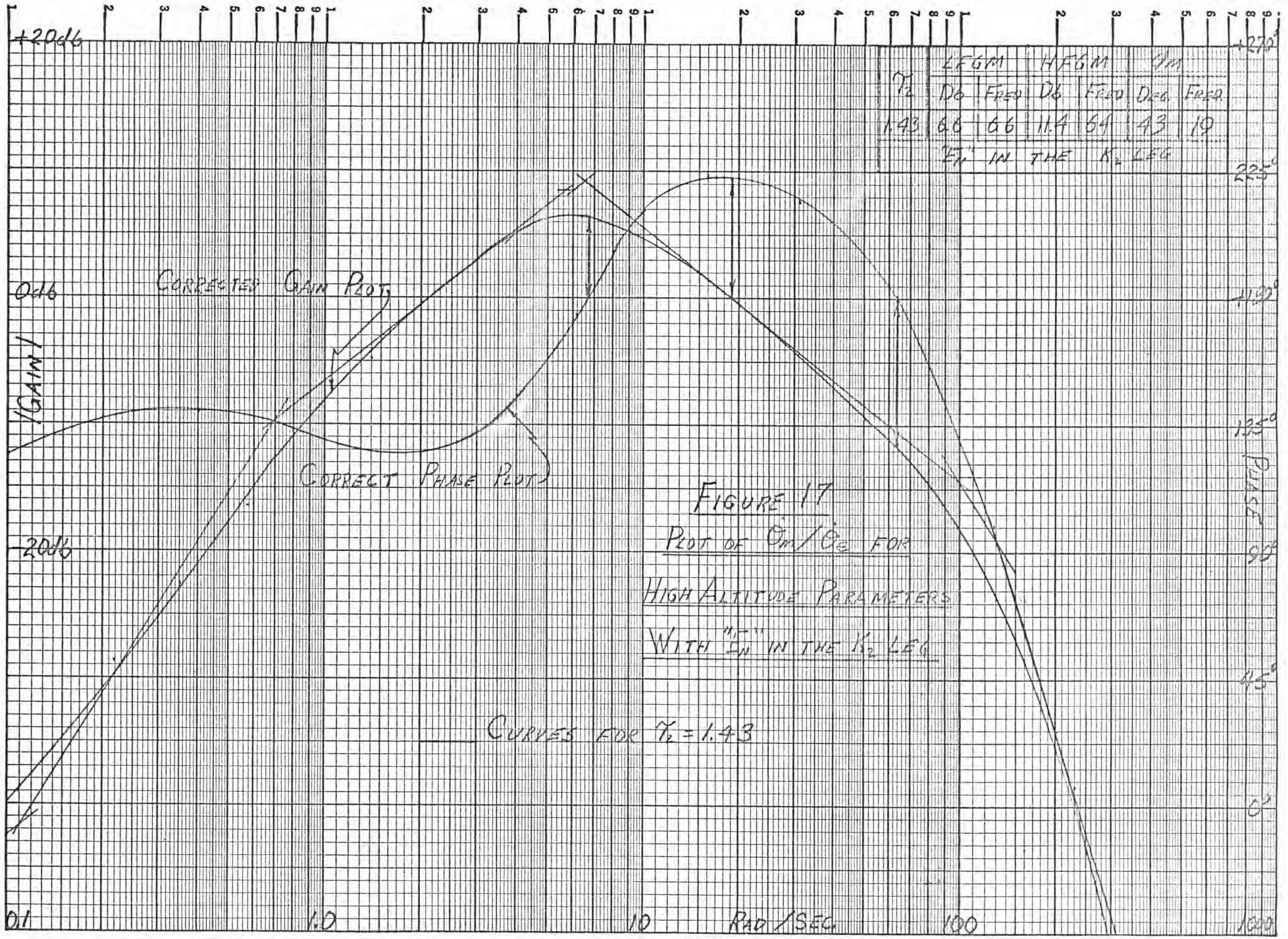
+20db
0db
-20db
GAIN
CORRECTED GAIN PLOT
CORRECT PHASE PLOT
+270°
225°
180°
135°
90°
45°
0°
PHASE
0.1
1.0
10
RAD/SEC
100
1000
LFGM
HFGM
ω_m
T_2
DB
FREQ
DB
FREQ
DEG
FREQ
1.43
66
66
11.4
64
43
19
"T_N" IN THE K_2 LEG
FIGURE 17
PLOT OF θ_m/θ_e FOR
HIGH ALTITUDE PARAMETERS
WITH "T_N" IN THE K_2 LEG
CURVES FOR $T_2 = 1.43$

satisfy the gain and phase margin requirements quite easily.

Table 2. Data from Bode Plots

Altitude	"E_N"	T_2	LFGM		HFGM		Phase Mar	
			Db	Freq	Db	Freq	Deg	Freq
Low	Out*	----	4.7	16.7	5.8	68	28	37
	$F_2(s)$ Leg	1.43	4.8	16.0	6.0	68	30	37
	K_2 Leg	1.43	5.0	16.1	6.2	66	29	37
High	Out*	----	6.4	6.8	11.3	65	43	20
	$F_2(s)$ Leg	1.43	6.3	6.5	11.4	68	45	20
	K_2 Leg	1.43	6.6	6.6	11.4	64	43	19

*"E_N" was out of the circuit

ANALOG SIMULATION APPROACH TO BIAS ELIMINATION STUDY

The second part of the analysis is the actual analog simulation of the autopilot to accomplish the following:

1. Verification of the calculated data.
2. Determination of a minimum value of T_2.
3. The study of the effects of the bias elimination scheme in the n_m transient response.

The analog block diagram for low and high altitude are shown in Figures 18 and 19. As shown, "E_N" is in the $F_2(s)$ leg in Figure 19 and in the K_2 leg in Figure 18. In order to simulate the present autopilot "E_N" should be replaced by one operational amplifier.

Table 3 lists the margins determined by analog simulation for different values of T_2 with "E_N" located either in the $F_2(s)$ leg or in the K_2 leg. A comparison of Tables 2 and 3 shows only a small tolerable difference and therefore would represent an analog verification of Bode plot results.

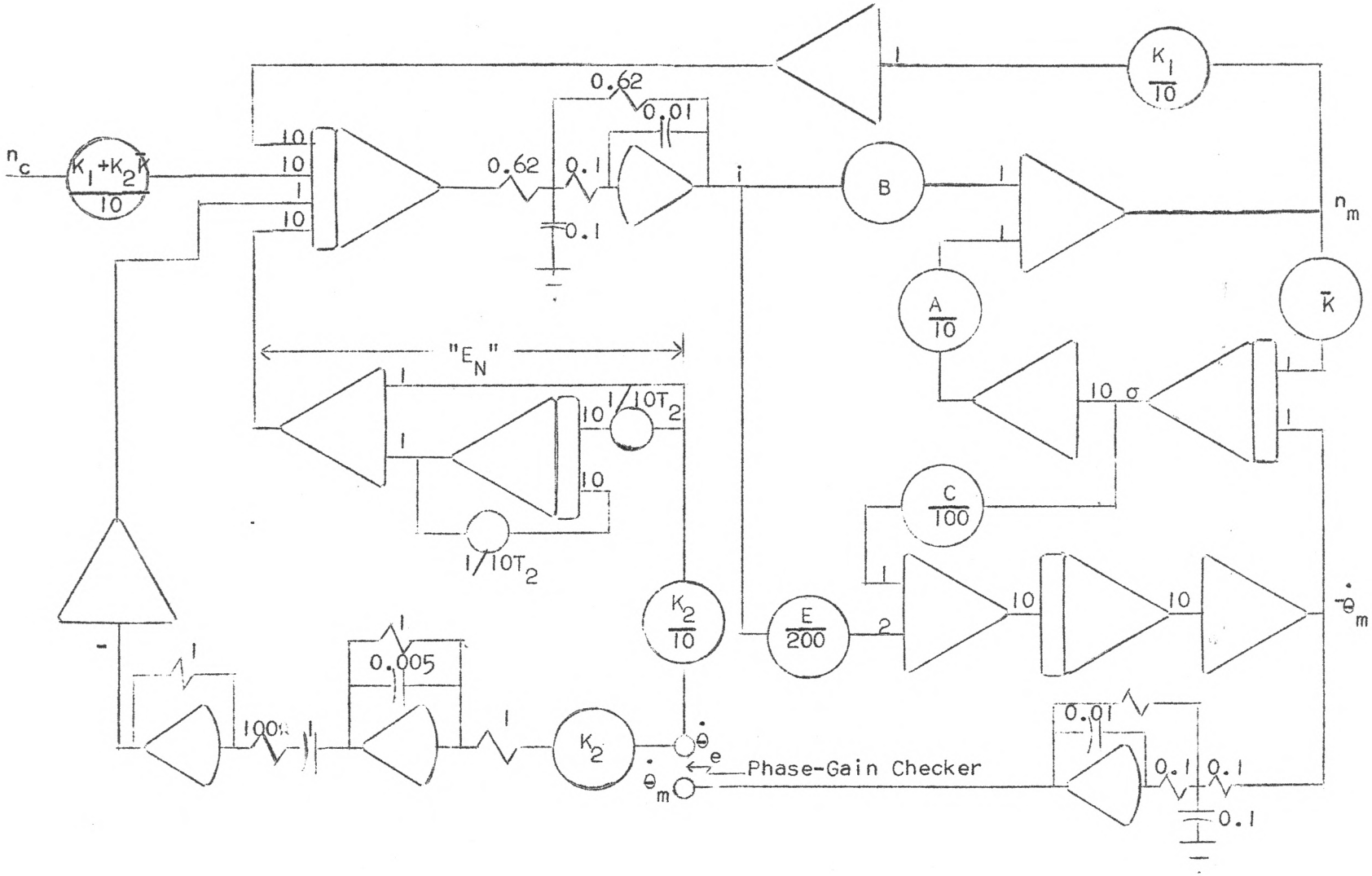

Figure 18. Computer Diagram For Basic Autopilot Scaled For Low Altitude Parameters

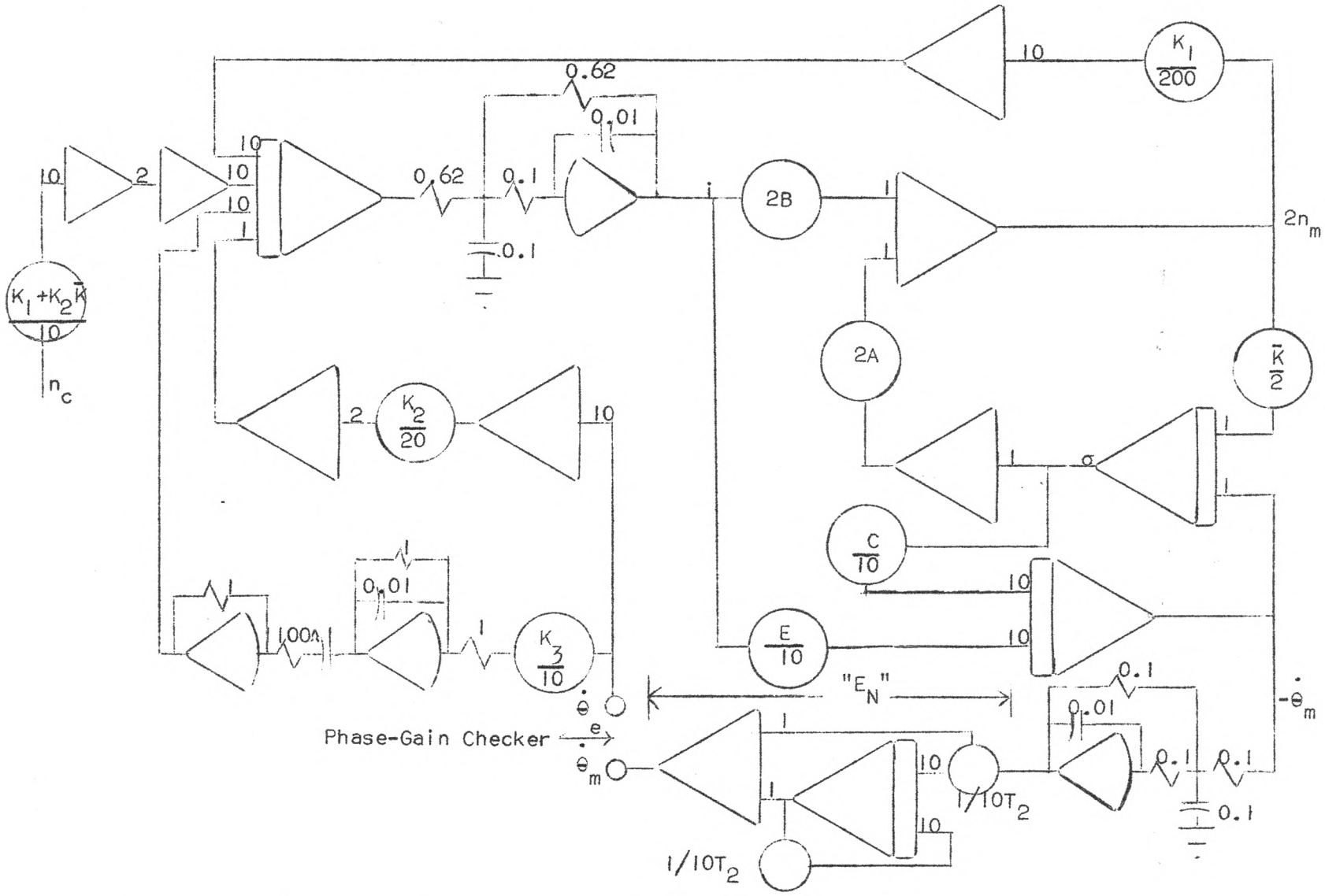

Figure 19. Computer Diagram For Basic Autopilot Scaled For High Altitude Parameters

Table 3. Data From Analog Simulation

Step No.	Alt.	Location of "E_N"	T_2	LFGM		HFGM		Phase mar.	
				Db	Freq.	Db	Freq.	Deg.	Freq.
1	LOW ALTITUDE	Out*	---	5.08	15.7	5.82	69	27.8	37.6
2		$F_2(s)$ Leg	2.5	5.00	15.7	6.08	72	29.4	34.5
3		"	1.43	5.06	15.7	6.10	72	30.0	34.5
4		"	1.0	5.12	15.7	6.14	72	30.6	34.5
5		"	0.4	5.20	15.7	6.24	72	33.0	34.5
6		K_2 Leg	2.5	4.80	15.7	6.24	66	30.8	37.6
7		"	1.43	4.84	15.7	6.24	66	30.8	37.6
8		"	1.0	4.92	15.7	6.24	66	30.8	37.6
9		"	0.4	5.28	15.7	6.24	66	31.8	38.9
10	HIGH ALTITUDE	Out*	---	6.38	6.8	11.3	66	40.6	18.8
11		$F_2(s)$ Leg	2.5	6.32	6.2	11.4	66	42.6	18.8
12		"	1.43	6.30	6.5	11.4	66	43.4	18.8
13		"	1.0	6.20	6.9	11.7	66	44.4	18.8
14		"	0.4	4.70	10.0	11.6	66	48.8	18.8
15		K_2 Leg	2.5	6.60	6.2	11.4	66	40.6	18.8
16		"	1.43	6.74	6.3	11.4	66	40.6	18.8
17		"	1.0	6.90	6.3	11.4	66	40.6	18.8
18		"	0.4	7.10	6.9	11.4	66	40.6	18.8

*"E_N" was out of the circuit

Several interesting items can be noted from Table 3. It appears that for a decreasing value of T_2 with "E_N" in the K_2 leg the margins go up and thus would yield a better and more stable system. This is not the case however as will be seen in the next section when the transient response is considered. This shows however that if the transient response is approximately the same for either location of "E_N" it would be more desireable to place it in the K_2 leg. The critical margin is found to be the LFGM since the addition of "E_N" has a much more pronounced effect on it. This can be seen from the Bode plots also and is due to the low frequency effect of the high pass filter.

The next phase of the analog computation and also the determining part of the analysis is the investigation of the transient effects of n_m for a step input of 1 g. These results are shown in Figures 20 through 29 along with $\dot{\theta}$, σ, and i. (Note: σ and α are synonymous).

These 10 Figures are divided into steps as shown in Table 3 and will be a sampling of the 18 steps shown their.

By looking at these Figures two distinct classifications are evident. For the low altitude condition all transient responses appear to have only a slight overshoot and are non-oscillatory for all values of T_2 chosen; however, the settling time is excessive for larger values of T_2.

The high altitude condition reveals a much different response. Remembering the original criteria of 20% maximum overshoot it is seen that a value of $T_2 = 1.43$ is the smallest value

of T_2 that will satisfy this criteria (Figures 26 and 28) and from Figures 27 and 29 for $T_2 = 0.4$ it is seen that a highly oscillatory response occurs. For a T_2 slightly less than 0.4 the system will go completely unstable.

For the low altitude response there is essentially no difference in response for either location of "E_N". The same holds true for the high altitude response.

Analyzing the two altitude responses it can be seen that it would be desireable to have the smallest possible value of T_2 (within limits of stability of course) for the low altitude condition and a value of T_2 as large as possible for the high altitude condition.

To arrive at a compromise value the first limitation is the 20% overshoot criterion for the high altitude condition. This establishes a value of T_2 no smaller than 1.43 and therefore becomes the value of $T_2 = 1.43$ as determined directly by the transient response. As was shown earlier this value of T_2 was used in the analytical approach and was found acceptable as far as the limiting criterion were concerned.

The only problem now remaining is the consideration of the time required to reach final value (settling time) which is evident at the low altitude transient response.

The larger the value of T_2 the longer the system will take to reach final value. This trend, as observed from the transient response, was verified analytically by taking a time solution of n_m / n_c. It was found that this effect was due to a slowly de-

caying exponential dependent on T_2 and due to the addition of the "E_N" network.

By observing Figures 21 and 23 it can be seen that the initial response rises to 80% of final value, decreases slightly to 75% of final value and then slowly approaches final value (approximately six seconds). The undesireability of this effect will be determined by each particular systems requirement. If the only requirement is that the system reach 63% of final value in a determined time then this system will be very satisfactory; but, if a final value time is very critical then this system may not be satisfactory. As in the case of an autopilot, if the system control signal (n_c) consists of many inputs in a short interval of time then the slower final value time would not be objectionable and just the initial rise time would be of interest.

CONCLUSION

For the addition of a decoupling circuit in either the K_2 leg or the $F_2(s)$ leg for the general autopilot described little difference in the gain and phase margins was noted between locations. However, for low altitude conditions better margins were recorded for the network in the $F_2(s)$ leg and for high altitude conditions better margins were recorded for the network in the K_2 leg. With a $T_2 = 1.43$, however, all margins satisfied the preliminary criterion.

The transient response for both locations of "E_N" showed approximately the same response for corresponding values of T_2.

This therefore means that basically either location of "E_N" would be acceptable. The engineer is now left with the problem of determining which location will best fit his particular application.

The question now is whether the addition of the "E_N" will introduce new factors which will degrade the system response. This question also will have to be left to the designer of a specific system. As was discussed in the last part of the analysis, specific system requirements will determine the acceptability of this type of rate gyro bias elimination.

This thesis is intended primarily as an introduction to an idea which can have much merit. Practically, the idea presented should be used only for preliminary study. For actual applications much further study is needed to justify the addition of such a network. One very encouraging item, however, is that with the studies just completed the probability of the success of such advanced studies appears very encouraging.

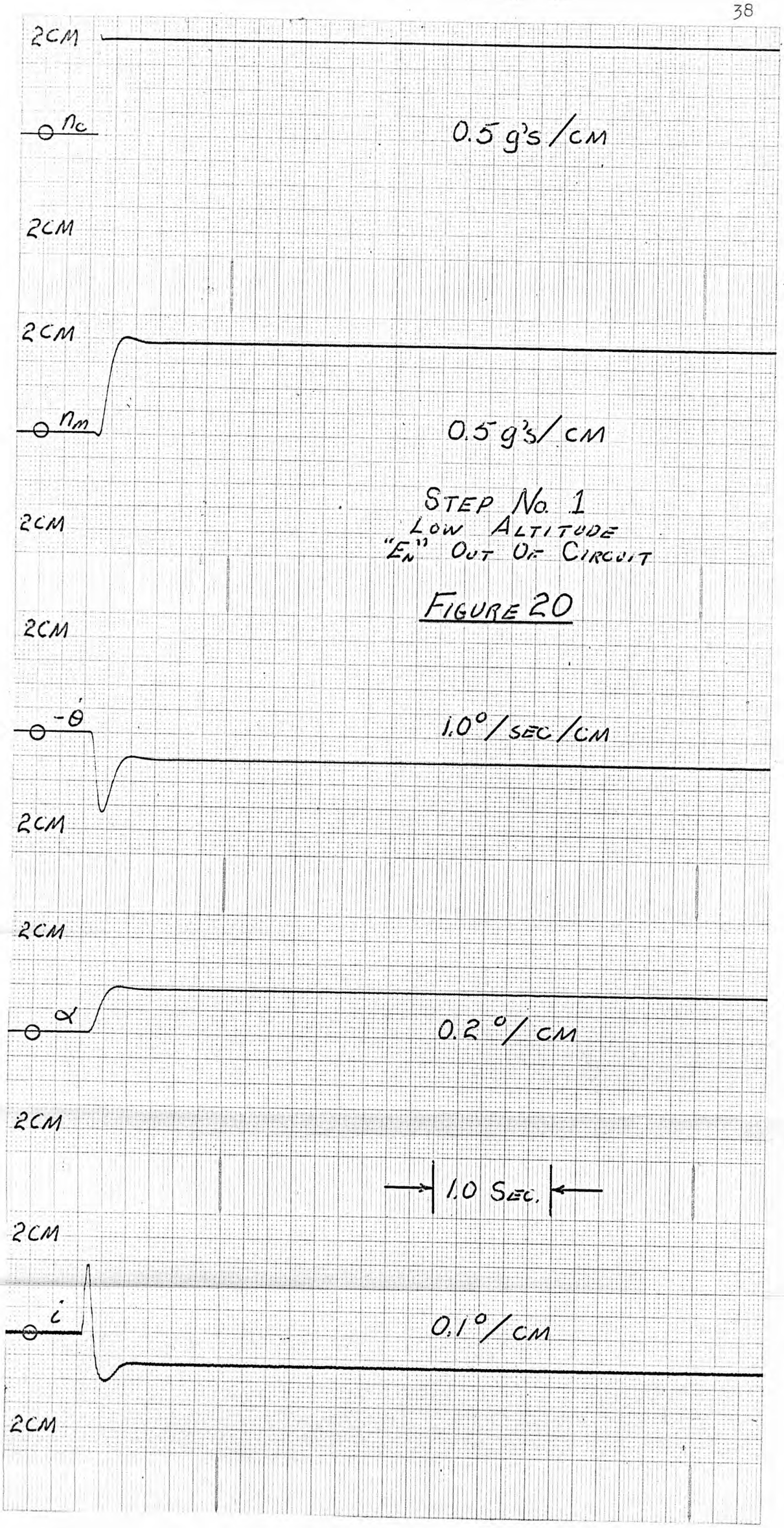

STEP No. 1
LOW ALTITUDE
"E_N" OUT OF CIRCUIT

FIGURE 20

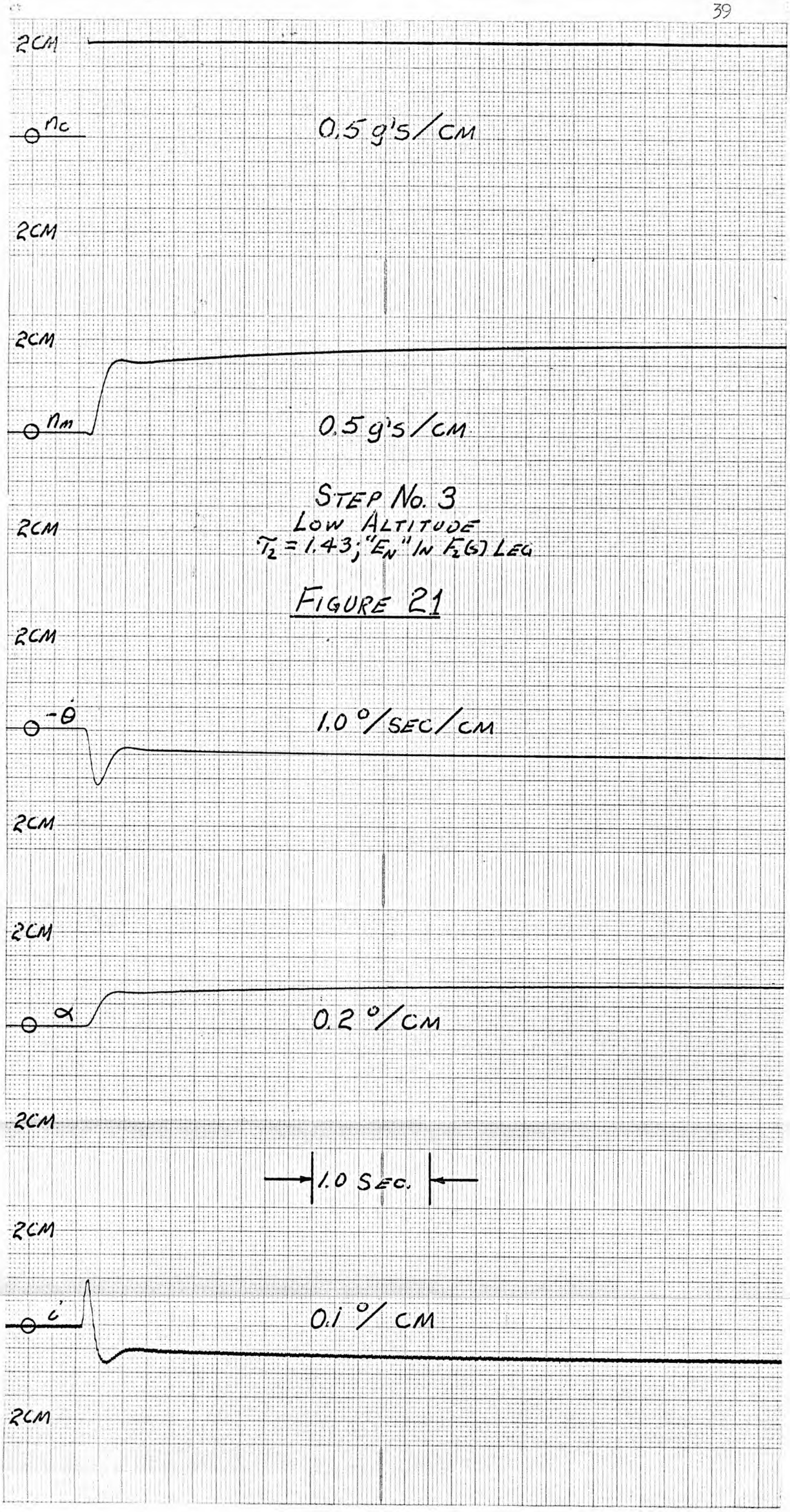

STEP No. 3
LOW ALTITUDE
$T_2 = 1.43$; "E_N" IN $F_2(G)$ LEG

FIGURE 21

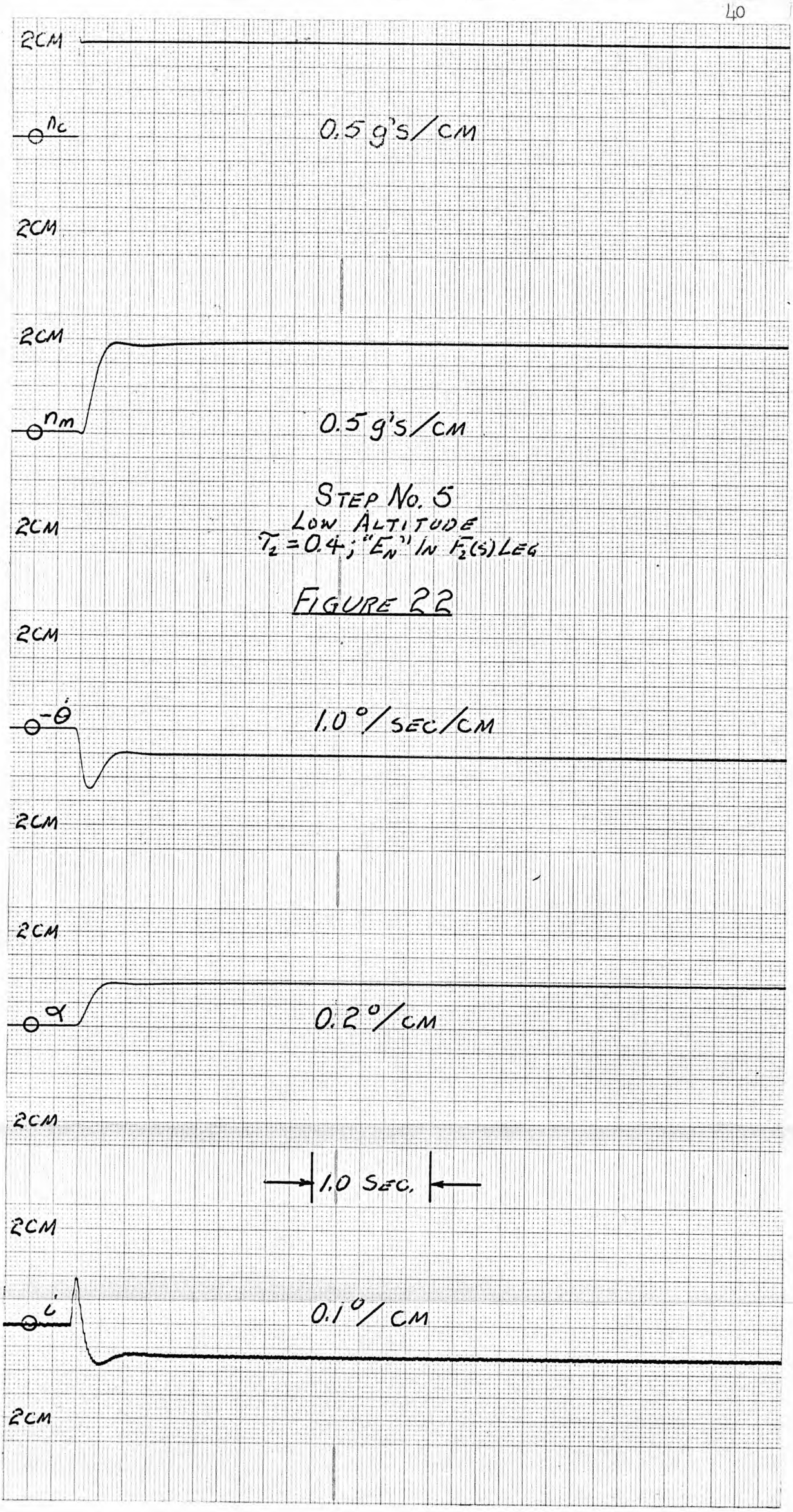

STEP NO. 5
LOW ALTITUDE
$T_2 = 0.4$; "E_N" IN $F_2(s)$ LEG

FIGURE 22

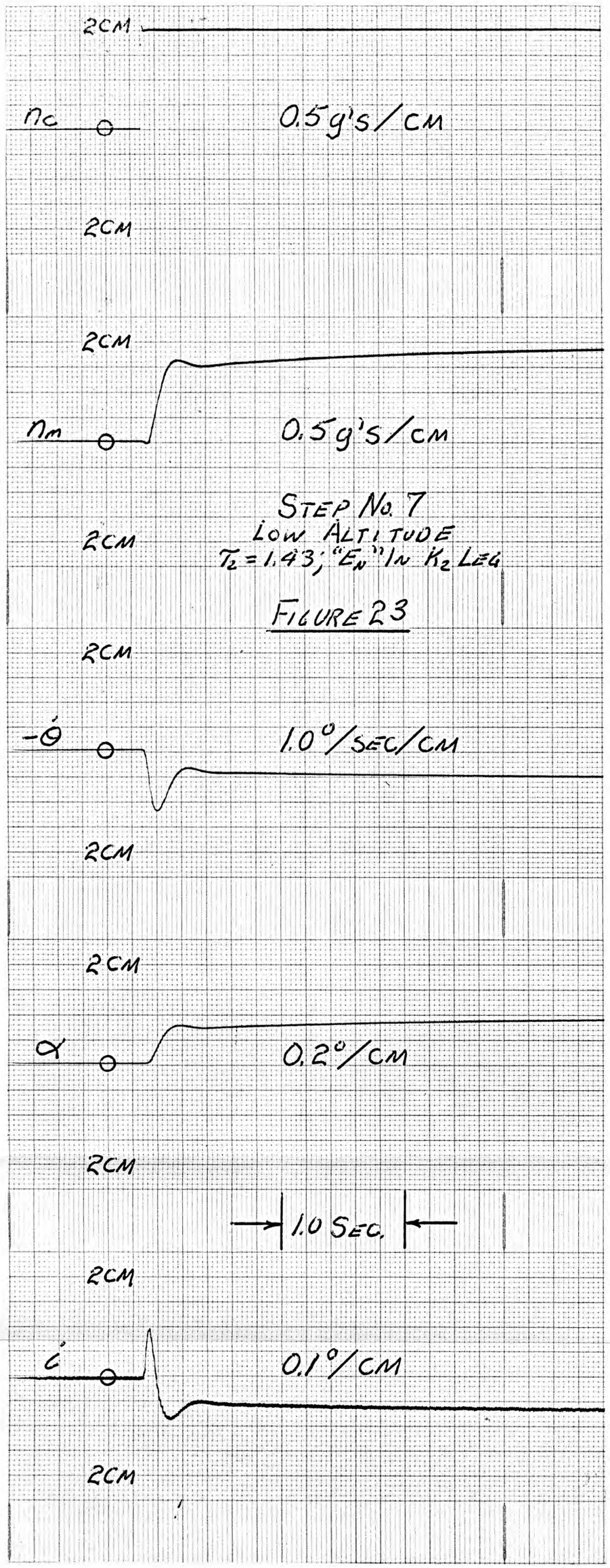

STEP NO. 7
LOW ALTITUDE
$T_2 = 1.43$; "E_N" IN K_2 LEG

FIGURE 23

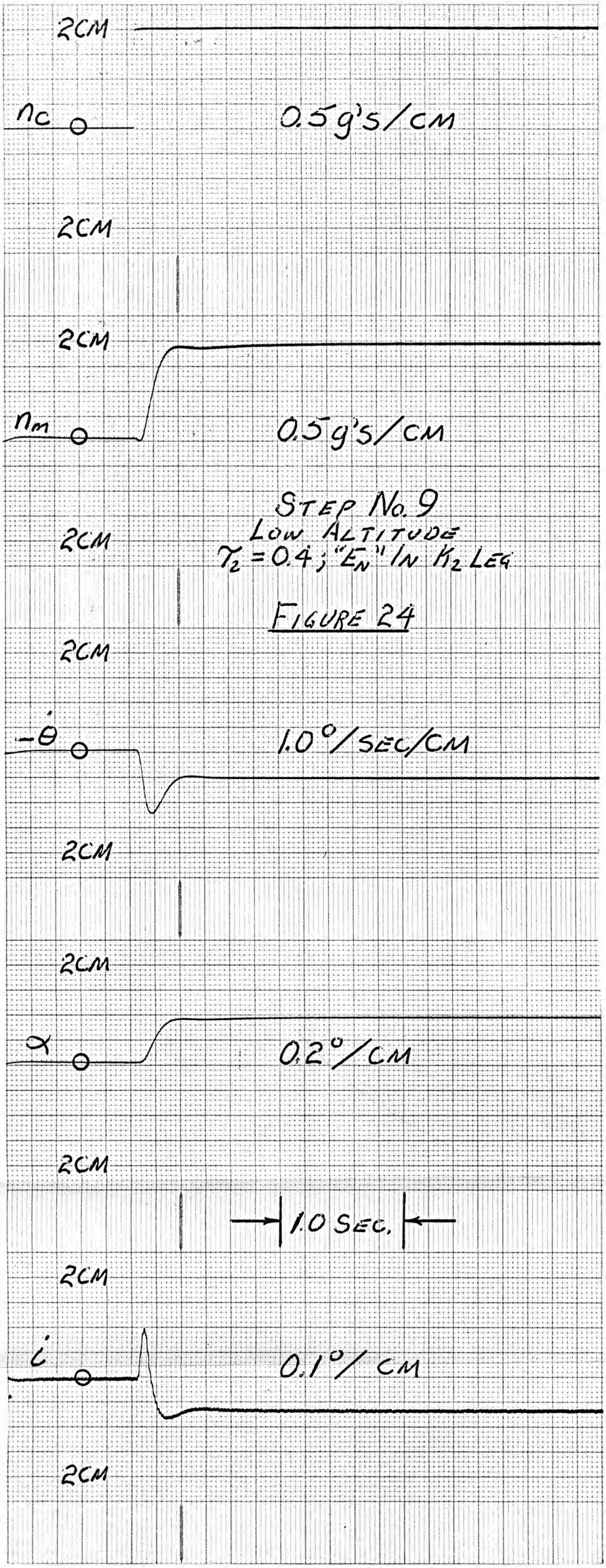
2CM
n_c
0.5 g's/CM
2CM
2CM
n_m
0.5 g's/CM
STEP No. 9
LOW ALTITUDE
$T_2 = 0.4$; "E_N" IN K_2 LEG
2CM
2CM
$-\dot{\theta}$
1.0°/SEC/CM
2CM
2CM
α
0.2°/CM
2CM
1.0 SEC.
2CM
$\dot{\iota}$
0.1°/CM
2CM

FIGURE 24

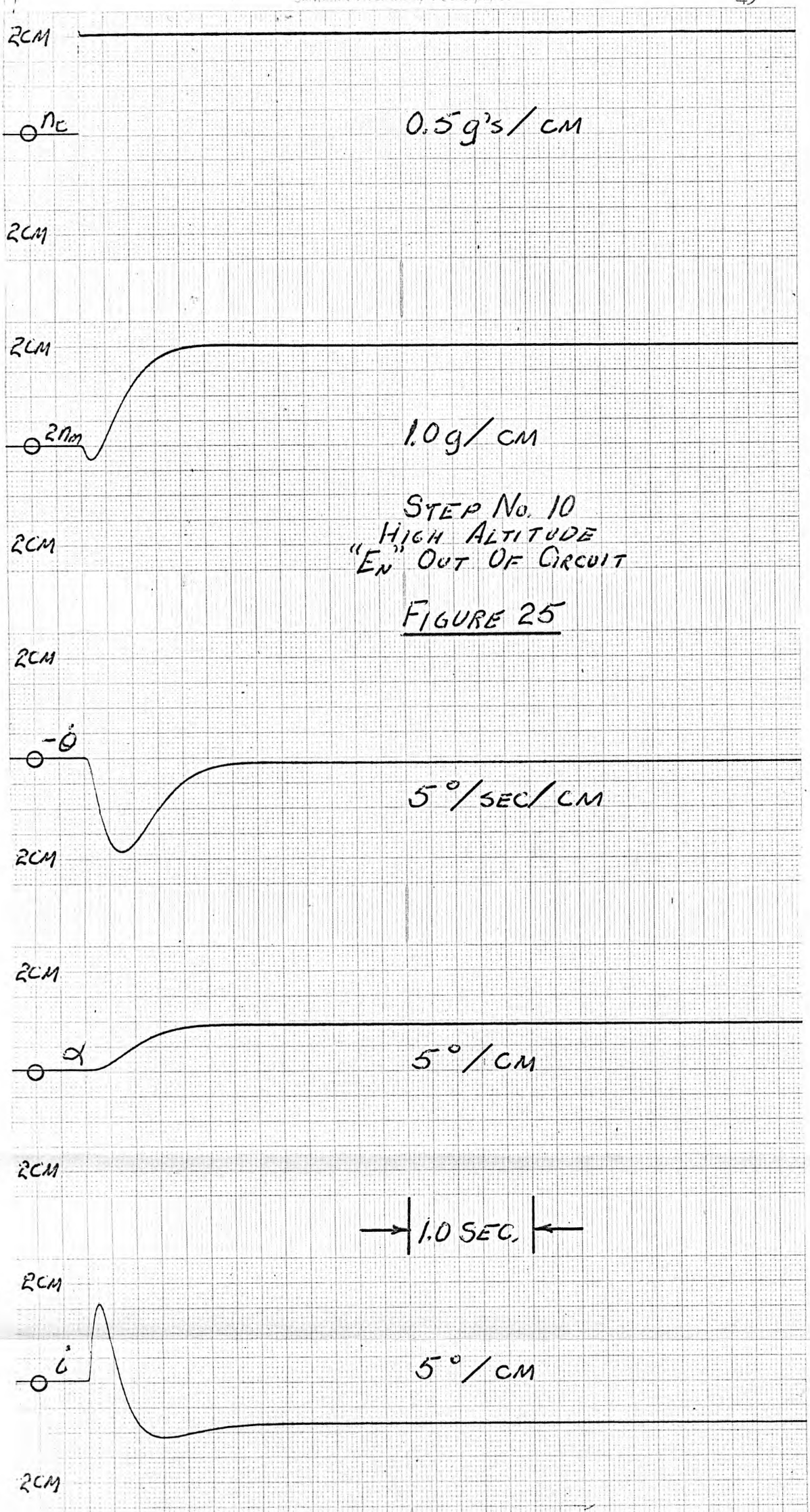
2CM
n_c
0.5 g's / CM
2CM
2CM
2nm
1.0 g / CM
2CM
STEP No. 10
HIGH ALTITUDE
"E_N" OUT OF CIRCUIT
2CM
$-\dot{\theta}$
5° / SEC / CM
2CM
2CM
α
5° / CM
2CM
1.0 SEC.
2CM
$\dot{\phi}$
5° / CM
2CM

FIGURE 25

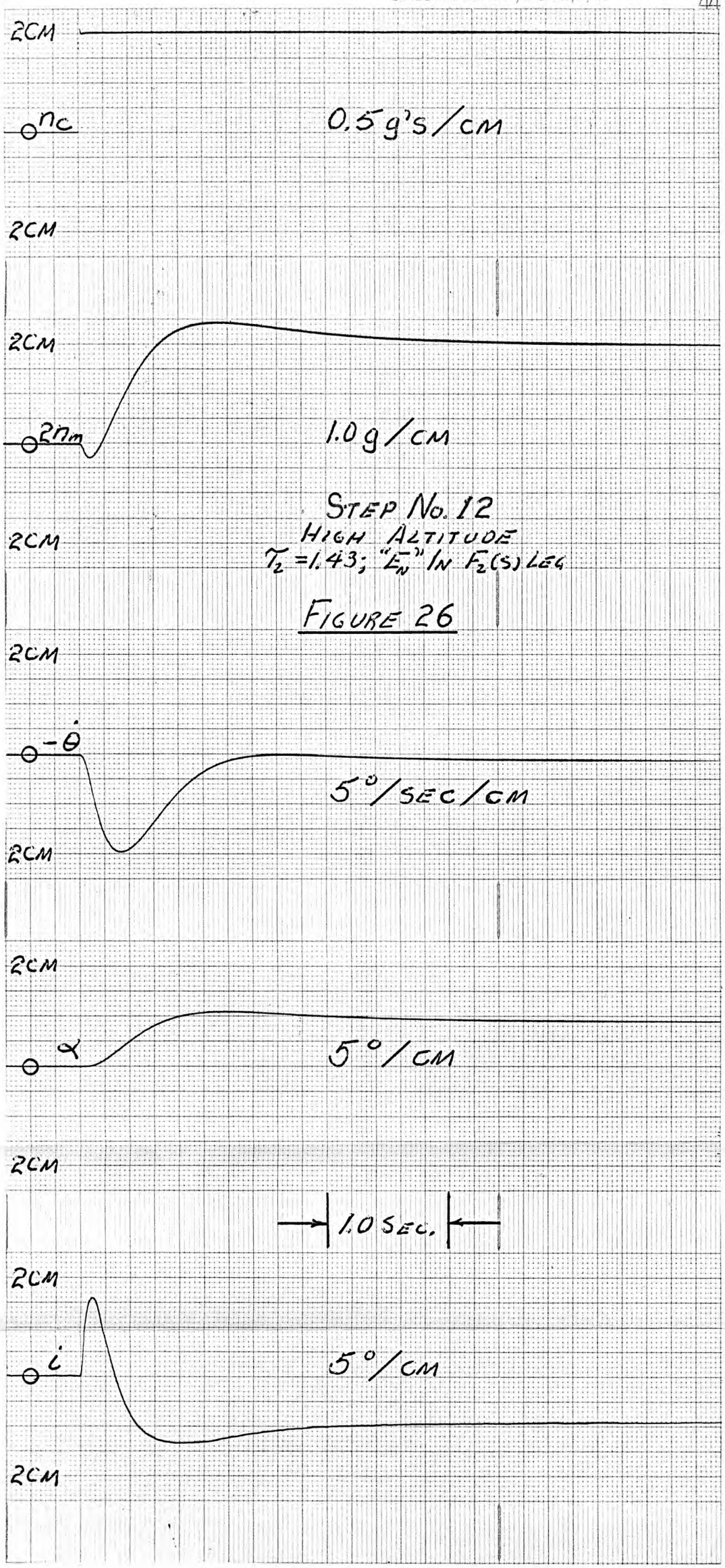

STEP No. 12
HIGH ALTITUDE
$T_2 = 1.43$; "E_N" IN $F_2(s)$ LEG

FIGURE 26

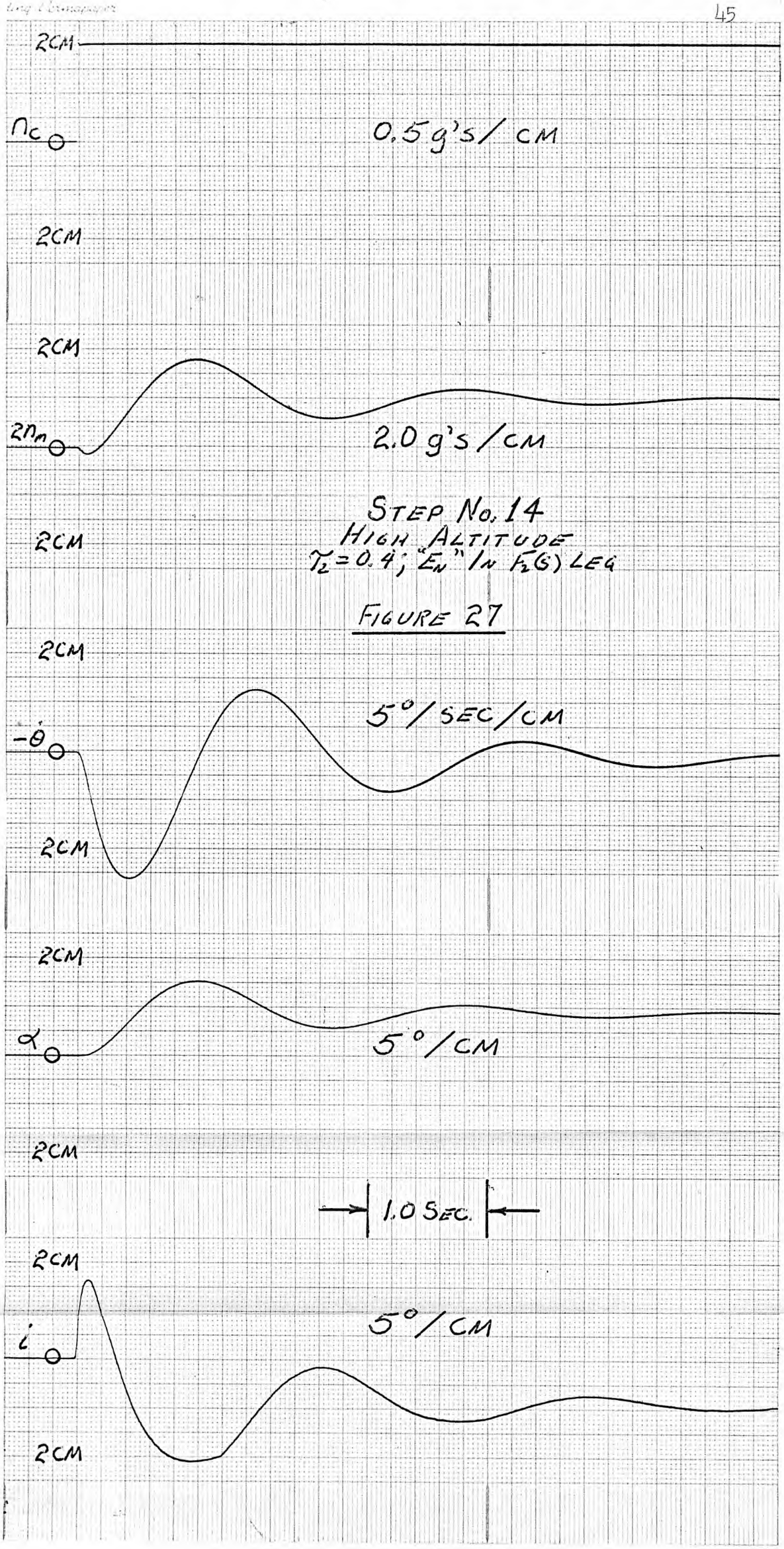

STEP No. 14
HIGH ALTITUDE
$T_2 = 0.4$; "E_N" IN $F_2(G)$ LEG

FIGURE 27

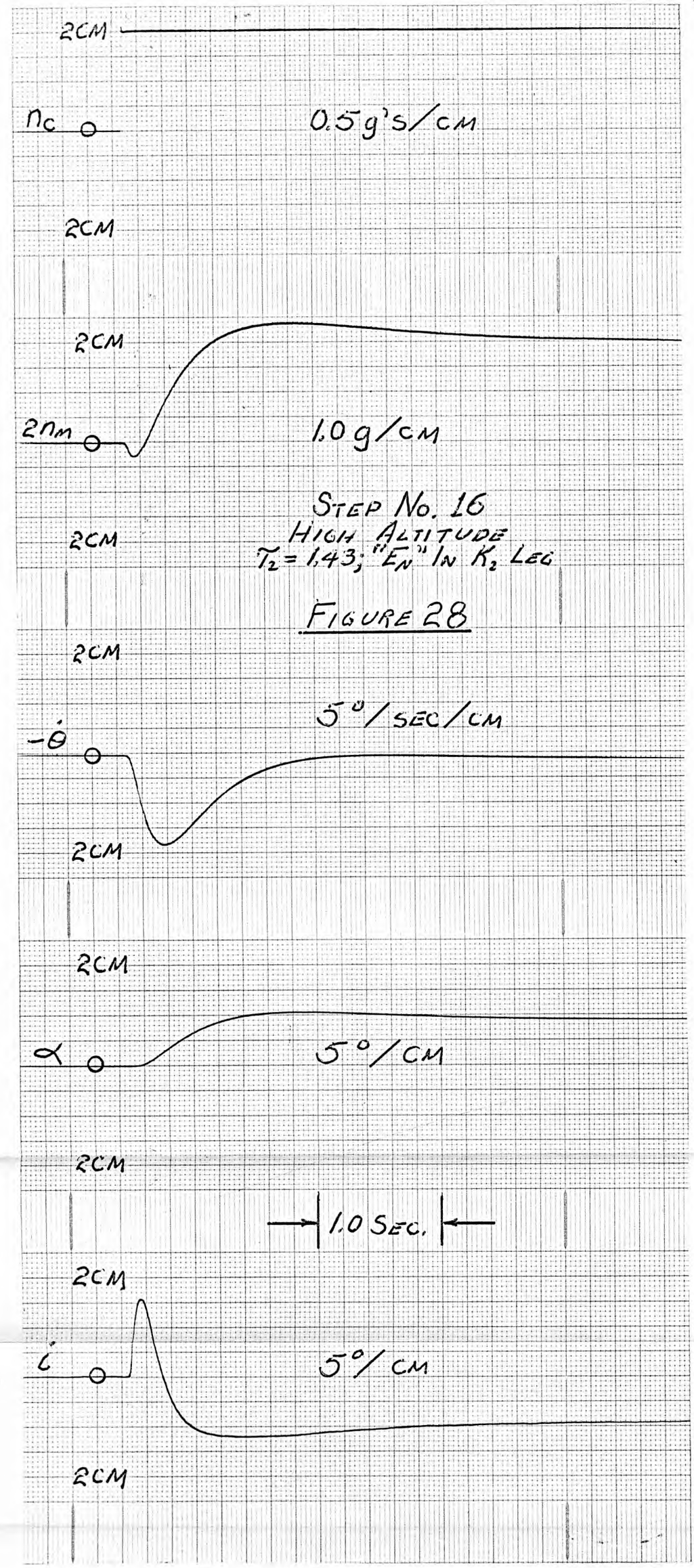

STEP NO. 16
HIGH ALTITUDE
$T_2 = 1.43$; "E_N" IN K_2 LEG

FIGURE 28

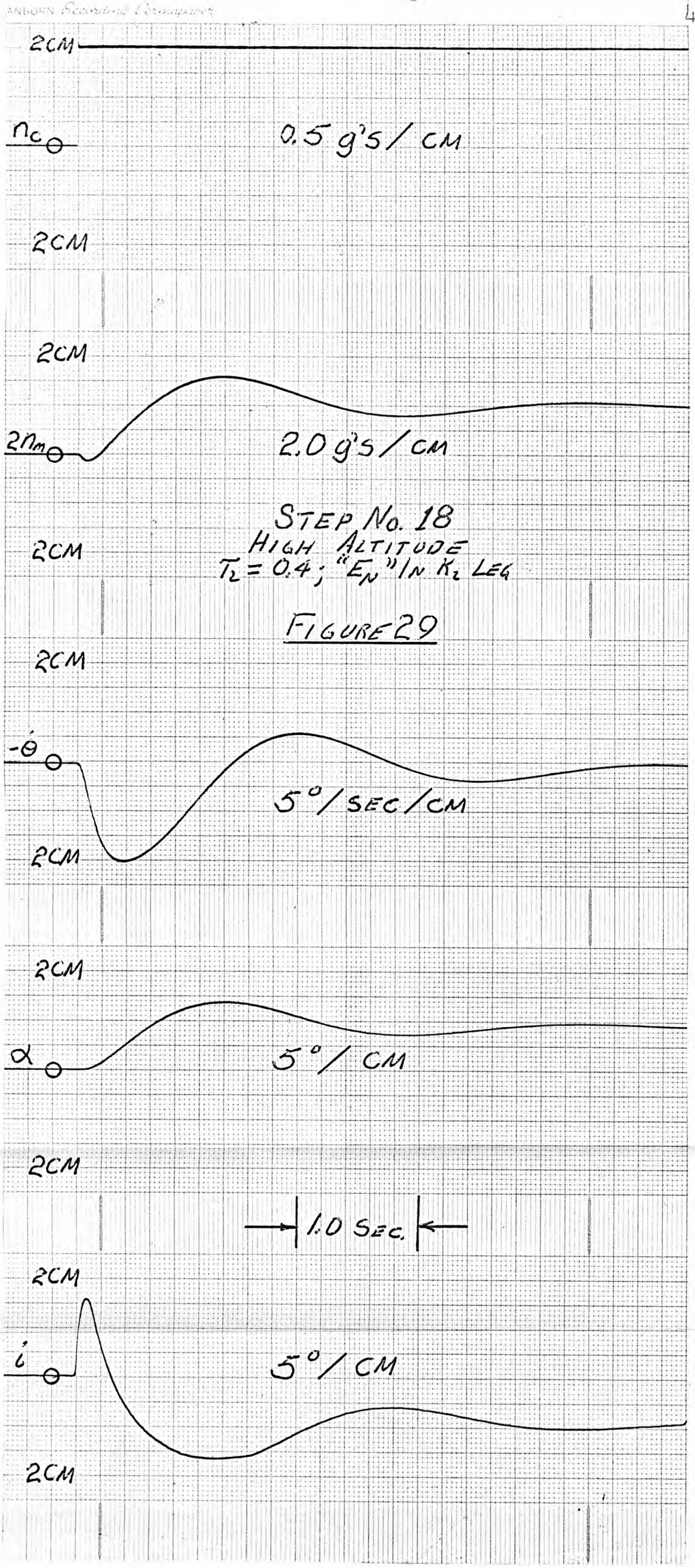

STEP No. 18
HIGH ALTITUDE
$T_2 = 0.4$; "E_N" IN K_2 LEG

FIGURE 29

ACKNOWLEDGMENT

The author wishes to express his sincere appreciation to his major instructor, Dr. Charles Murrish, for his interest and continual help and advice throughout the preparation of this thesis.

The author would also like to acknowledge the help rendered by members of the staff of Johns Hopkins University Applied Physics Laboratory. In particular the author would like to express his appreciation to Mr. Kenneth Duning who contributed the idea of this thesis and who gave continual guidance throughout the investigation of this thesis topic.

ANALYTICAL STUDY OF A TECHNIQUE FOR THE ELIMINATION OF STEERING RATE GYRO BIAS IN A TYPICAL MISSILE AUTOPILOT

by

ROBERT CLAYTON ESLINGER

B. S., Kansas State University
of Agriculture and Applied Science, 1962

AN ABSTRACT OF
A MASTER'S REPORT

submitted in partial fulfillment of the

requirements for the degree

MASTER OF SCIENCE

Department of Electrical Engineering

KANSAS STATE UNIVERSITY
Manhattan, Kansas

1963

Approved by:

C. H. Murrish

Major Professor

In many missile autopilots rate gyro feedback is used to help stabilize the system. Associated with the rate gyro is a steady state bias which can be large enough to have a pronounced effect on missile performance. This bias will vary, of course, with the quality of gyro but if an inexpensive means could be developed to alleviate the bias problem considerable savings could be effected through the use of lower quality gyros.

The purpose of this thesis is to show a means of decoupling this gyro bias and then to investigate the system to make sure missile autopilot performance is not depreciated significantly.

The development of a typical autopilot is first undertaken and from this development it is proposed that a decoupling network be added in one of two places associated with the rate feedback loop. A lag network with a transfer function of $Ts / (Ts + 1)$ was chosen for this purpose and the system was analyzed for both locations of the network to determine if the original system response was altered.

An analytical study of the system was first undertaken and Bode plots were made to determine the gain and phase margins for the present system and for the compensated system for different values of T. An analog simulation was made to determine the transient response, to verify the analytical results, and to choose the best value of T.

From these studies it appears that a decoupling process of the type described and a value of $T = 1.43$ would be possible but would depend largely on the particular system and its requirements. The biggest problem is that of the settling time or that time

required for the system to reach final value. For a particular system this problem would have to be investigated further.

This thesis is intended primarily as an introduction to an idea which can have much merit. Practically, the idea presented should be used only for preliminary study. For actual applications much further study is needed to justify the addition of such a network. One very encouraging item, however, is that with the studies just completed the probability of the success of such advanced studies appears very encouraging.